University of Stavanger

FACULTY OF SCIENCE AND TECHNOLOGY

MASTER'S THESIS

Study programme/specialisation: Petroleum Engineering, Natural gas Engineering	Spring semester, 2021 Open
Author: Kwaku Ennin Afoakwa	Author's signature
Supervisor: Zhixin Yu	
Title of master's thesis: Dry reforming of methane over Ni-Fe bimetallic catalyst	
Credits: 30 ECTS	
Keywords: Dry reforming of methane Synthesis gas Heterogeneous catalyst Hydrotalcite Co-precipitation Catalytic activity	Number of pages: 53 Stavanger, 15th June 2021

ACKNOWLEDGEMENT

Now thank we all our God, with heart and hands and voices, who has done wondrous things and in whom we rejoice. First and foremost, I would like to thank God Almighty for His goodness and mercy upon my life and His constant guidance.

To my supervisor Professor Zhixin Yu who has been my mentor throughout this period of writing my thesis I would like to express my profound gratitude. Thank you for your motivation and guidance.

Also, I would like to thank Huong Lan Huynh, Song Lu and all the Engineers of the Department of Energy and Petroleum Engineering for your support and assistance in the laboratory. I have learnt so many things during this period and I am really grateful for your help.

Special thanks to my friends, family, and the Church of Pentecost International Norway for the moral, physical, mental, and spiritual support for the past 2 years in Stavanger. Especially my Mum, Maa Mary, Efua Ansah, Victoria, Priscilla, Solomon, Iyad and my lovely sister Ennin Afua Ampofowaa. Words alone cannot describe my heartfelt gratitude to you all for the love you have shown me. Nyame nhyira mo bebere.

Lastly, to my classmates the battle has finally ended, and we all made it. Thank you very much for your help, love and all the memorable times we shared together.

ABSTRACT

Our climate is changing for the worse as the concentration of greenhouse gases in the atmosphere increases. Climate change is one of the most important challenges of our time. Emissions of greenhouse gases (GHG) have been rising steadily since the industrial revolution because of the increased use of fossil fuels. Today, there is a well-established scientific link between the concentration of GHG in the atmosphere and the average temperature on earth. Much research has been conducted to study how effectively these emissions can be reduced drastically. Among many others, one way of doing that is the utilization of the CO_2 by reforming of methane to produce synthesis gas which can be valorised in the production of several chemicals such as methanol, ammonia, synthetic gasoline.

Heterogenous catalyst is mostly used for dry reforming of methane (DRM). Developing a stable, active, and cheap catalyst is being a major obstacle in the industry for a long time. Bimetallic Ni-Fe catalysts derived from hydrotalcite materials have been reported to be promising for the DRM reaction. The hydrotalcite (HT) materials possess high surface areas, high thermal stability, and uniform distribution of active metals.

This thesis focuses on the study and synthesis of several bimetallic Ni-Fe HT derived catalyst with Fe/Ni molar ratio ranging from 0.05 to 0.3. In each of these catalysts, the Ni loading remained constant at 20 wt.%. After the preparation of these catalysts, they were characterized by X-ray diffraction (XRD), nitrogen adsorption-desorption, temperature programmed reduction (TPR) and temperature programmed desorption (TPD).

Preparation was carried out using co-precipitation at high supersaturation method followed by calcination. All of the catalysts showed promising results, the hydrotalcite-like materials were successfully achieved and were confirmed by XRD patterns.

The catalytic activity of each of the samples prepared was studied in a DRM reaction at 700 ^oC in a fixed bed reactor. With a gas hourly space velocity (GHSV) of 300,000 $mLg^{-1}h^{-1}$, the catalyst with the Fe/Ni molar ratio of 0.15, CAT-0.15 was determined as the best sample due to its high conversions and stability. The final CH_4 and CO_2 conversions of this catalyst were 52% and 65% respectively and a final H_2/CO of 0.76. The catalyst remained stable for the whole 24 h period of the reaction.

TABLE OF CONTENT

LIST OF TABLES

LIST OF FIGURES

1. INTRODUCTION

1.1 Background

In recent times, the eagerness to find a long-lasting solution to the rapid emissions of CO_2 into the atmosphere has increased significantly. This is because of the established scientific relationship between CO_2 emissions, the average global temperature and climate change. This led to about 195 countries adopting the Paris Agreement in 2015 to limit the average global temperature below 2 ^oC by 2050 [1].

In 2020, the average global CO_2 emissions dropped by approximately 26 Gt. This can be attributed to the increase in the global use of renewable energy. In the first quarter of 2020, the use of renewable energy in all sectors increased by 1.5% relative to 2019. Even though the use of renewable energy has increased, there is still a large percentage utilizing fossil fuels to meet their energy needs which produces huge emissions of carbon dioxide. The development of carbon capture and utilization (CCU) technologies has been described as one method to mitigate this challenge. These technologies focus on converting captured CO_2 into synthetic fuels and commodity chemicals [2].

DRM has been considered as an approach to valorise CO_2 to produce synthetic gas (syngas) with H_2/CO ratio of unity. This method has the potential not only to alleviate the environmental issues surrounding GHG emissions but also suitable for Fischer Tropsch synthesis (FT) [3]. The use of appropriate downstream processes accompanied with controlled FT conditions produces high yield of gasoline, excellent quality diesel fuel, or high value linear α-olefins [4].

After nearly three decades of intensive research, nickel-based catalysts have been identified as the most suitable alternative to noble metal-based catalysts because of their low cost, availability, and high initial activity [5]. Despite the pros listed above, there are some cons with these catalysts. Ni-based catalyst for DRM reaction undergoes quick deactivation due to carbon formation and sintering.

However, the introduction of suitable support to Ni-based catalyst has the propensity to improve the catalytic activity and reduce coke formation in DRM reaction [6]. In selecting the best support for an active site, high specific surface area, high thermal stability and good basicity are few qualities which are taken into consideration. This has made γ-Al_2O_3 one of the most studied supports for nickel because it possesses these qualities [7]. Combining γ-Al_2O_3 and MgO as mixed oxides supports has been reported to increase the basicity, specific surface area and total

pore volume [8]. Then again, a compelling approach considering bimetallic catalyst has been proposed as of late to improve stability and activity.

The catalytic properties in a DRM reaction are affected by the methods used for the catalyst synthesis. Hydrotalcite-like materials have presented itself as a suitable catalyst precursor for DRM reaction basically because it creates an opportunity to synthesize a homogeneous material consisting of Ni, MgO and Al_2O_3. These homogeneous mixed oxides with high surface area and thermal stability are formed after controlled thermal decomposition. Subsequently they become small and stable metal crystallites upon further reduction.

1.2 Scope of the study

The aims of this master's thesis were to:

- Prepare a series of bimetallic Ni-Fe HT with Fe/Ni ratio from 0.05 to 0.3 using coprecipitation at high supersaturation by the so-called fast injection method.
- Characterize the catalyst by X-ray diffraction (XRD), nitrogen adsorption-desorption, temperature programmed reduction (TPR) and temperature programmed desorption (TPD)
- Test catalysts in DRM reaction at a temperature of 700 ^{o}C, atmospheric pressure and a gas hourly space velocity (GHSV) of 300,000 $mLg^{-1}h^{-1}$.
- Test best catalyst in DRM reaction at different temperatures, atmospheric pressure, and a gas hourly space velocity (GHSV) of 300,000 $mLg^{-1}h^{-1}$.
- Long term catalytic activity test for the best catalyst

2 LITERATURE REVIEW

2.1 Thermodynamics of Dry Reforming of Methane

The DRM is a chemical process that consists of converting methane and carbon dioxide, identified as the world's most abundant greenhouse gases, to syngas (hydrogen and carbon monoxide), with a H_2/CO molar ratio of 1. But the H_2/CO ratio could be modified through the water gas shift reaction to obtain a desired ratio of 2 for methanol synthesis [9]. The first investigations concerning converting CO_2 and CH_4 into synthesis gas were reported in 1888. The process was further investigated by Fischer and Tropsch in 1928. Thus, DRM process is not a new concept.

Table 2.1 Main and side reactions of DRM

Reactions	**Equations**	ΔH_{298K} (kJ/mol)	T(^{o}C) $\Delta GT \leq 0$
Dry reforming of methane	$CH_4 + CO_2 \leftrightarrow 2CO + 2H_2$	+247	≥ 643
Reverse water gas shift	$CO_2 + H_2 \leftrightarrow CO + H_2O$	+41	≥ 827
CH_4 decomposition	$CH_4 \leftrightarrow C + 2H_2$	+75	≥ 546
CO disassociation (Boudouard reaction)	$2CO \leftrightarrow C + CO_2$	-171	≤ 703
CO_2 gasification	$C + CO_2 \leftrightarrow 2CO$	+171	≥ 703
Carbon water reaction	$C + 2H_2O \leftrightarrow 2H_2 + CO$	+90	≥ 631

The main reaction for DRM is endothermic as seen from the Table 2.1 [10]. From thermodynamic point of view, the reaction needs more of energy input compared to steam reforming and autothermal reforming. From calculations, this reaction only occurs spontaneously at temperatures above 643 ^{o}C. Also, there are several other side reactions possible to occur during the DRM process.

Coke is an undesired product in the DRM process because it hinders the catalyst activity by causing physical blockage of the reformer tubes, the disintegration of the catalyst support, compaction of metal crystals and pore blockage [11].

Methane decomposition and CO disproportionation are the two main reactions responsible for carbon formation during DRM. However, Nikoo and Amin [12] reported that hydrogenation of

carbon and hydrogenation of CO can also cause carbon/coke formation. The formation of coke from hydrocarbons takes place when there is decomposition on the metal surface of late transition metals such as nickel [13]. There are different types of carbon that can be formed based on the surface sites and reaction routes [14]. It is important to note that there is another side reaction called RWGS which is responsible for a H_2/CO ratio less than unity. Performing DRM outside the temperature ranges at which these reactions occur is effective to prevent carbon formation. Wang et al. [15] stated that the RWGS and Boudouard reactions will not occur at temperatures exceeding 820 ^oC.

Apart from conducting the reaction at elevated temperatures, the addition of alkali metal oxide promoters, basic supports and Ni alloying helps to attenuate the formation of carbon [16].

Even though, there have been many progresses and significant achievements for high temperature DRM, there is currently an intense research into DRM reactions at low temperatures (below 700 ^oC). Based on the detailed theoretical thermodynamic calculations of DRM reaction reported by Nikoo and Amin [12], when the DRM reaction at 300 ^oC reached equilibrium, the conversion of CH_4 and CO_2 were approximately 60% and 50% respectively. Even at 100 ^oC, hydrogen could be produced while CO might be generated when the temperature reaches 300 ^oC. This indicates the possibility of DRM reaction occurring at low temperatures with an efficient catalyst.

2.2 Catalysts for Dry Reforming of Methane

The development of an extremely active and stable catalyst with resistance against deactivation and economic feasibility is necessary for an effective industrialisation of the DRM process [9]. This has been a major area of research over the past ten years. Formation of catalytic coke, sintering of active material and oxidation of metallic active sites are the main cause of deactivation of DRM catalyst [7]. This chapter discusses major advances in DRM catalyst with respect to materials, preparation methods, supports, and promoters.

Iron, cobalt, nickel, ruthenium, rhodium, palladium, osmium, iridium, and platinum belonging to the transition metals of group 8, 9 and 10 of the periodic table have been reported as the active materials for DRM reaction. Noble metals are highly active and stable for DRM with high resistance to carbon formation and are capable of dispersing on their support and maintain a small particle size [3]. Ni- and Co-based catalysts are studied because they are relatively cheap and readily available. These catalysts exhibit activity like that of noble metal-based catalysts but quickly deactivate owing to either carbon formation or sintering [9].

2.2.1 Nickel Based Catalyst

Nickel based catalysts are the most frequent catalyst used at industrial scales since it is cheaper and readily available with good catalytic performance [17]. Due to its high endothermic nature, DRM needs high reaction temperatures. This leads to a serious problem called sintering, as the Tammann temperature of nickel is equal to 581 ^{o}C. This also speeds up the deactivation process through coke deposition [18]. The tendency of carbon formation on Ni catalyst can be lowered by using supports or promoters exhibiting strong Lewis basicity, addition of noble metal, sulphur passivation of Ni catalyst [19].

2.2.2 Catalyst Support

Generally, a catalyst is composed of more than one component, where these components are designed to the desired shape and structure. These support materials play vital roles in the enhancement of catalytic activity and reduction of catalyst deactivation through coke formation and active metal sintering especially at high temperature DRM. It also provides large active surface area [20]. Supports are most often dormant in catalytic reactions. However, supports with large surface area make the dispersion and embedding of active metals easier [17].

Many Ni-based catalysts on several supports have been tested in DRM reaction by many researchers. Some of these supports are single oxides (Al_2O_3, MgO, CeO_2, ZrO_2, mixed oxides (MgO-Al_2O_3, CeO_2-ZrO_2, CeO_2-Al_2O_3), zeolites, montmorillonite, carbon-based materials (carbon nanotubes, activated carbon).

One of the most studied supports for nickel catalysts is alumina. Comparatively, it is cheaper and possesses high specific surface area, basic character and some phases possess high thermal stability. But it is important to note that the catalytic properties of the catalyst in DRM reaction and its resistance to carbon formation depends on the catalyst structure, composition, calcination conditions and preparation method [7].

Guo et al. [21] compared the performance of Ni/γ-Al_2O_3, Ni/MgO-γ-Al_2O_3 and Ni/$MgAl_2O_4$ in dry reforming of methane. It was reported that the Ni/MgO-γ-Al_2O_3 and Ni/$MgAl_2O_4$ catalysts showed superior activity and stability over their counterpart when the stoichiometric feed ratio (1:1) was used. The combination of MgO to Al_2O_3 also helps to obstruct the formation of $NiAl_2O_4$ spinel phase which is inactive and leads to low metal dispersion of NiO/Al_2O_3 [22].

It is important to note that the catalytic properties of the catalyst in DRM reaction and its resistance to carbon formation depends on the catalyst support preparation method. A

comparison was made by Kim et al. [23] between impregnated Ni/γ-Al_2O_3 catalyst and Ni supported on alumina aerogel prepared by sol-gel method. When tested in a DRM reaction, the Ni supported on alumina aerogel was stable for 30 h time on stream (TOS) as compared to 4-5 h TOS of Ni/γ-Al_2O_3. This was attributed to the fact that the catalyst prepared by sol-gel method showed very high specific surface area, high porosity, and small distribution of metal particles.

2.2.3 Bimetallic nickel-based catalysts

These catalysts have been studied for DRM reaction since it is said to influence the catalytic structure and consequently the catalytic activity. Besides the noble metals, transition metals such as iron, copper, and cobalt have mostly been investigated as bimetallic system with Ni-based catalyst for DRM reaction.

Iron has become the best candidate (economically) to improve Ni-based catalyst for the reaction because it is cheaper compared to other transition metals [17]. Most of these Ni-Fe bimetallic catalysts are derived from specific structure like perovskite and hydrotalcite (HT). Most researcher reported that the catalytic activity depends on the Ni/Fe molar ratio.

Song et al [24] synthesized a porous monometallic Ni/Al_2O_3 and bimetallic NiFe/Al_2O_3 with a high surface area for low temperature DRM reaction. It was concluded that the latter enhanced CH_4 and CO_2 conversion and resistance to coking. Also, Ray et al in their work reported that by substituting Ni with Fe (Fe/Ni = 1/3), the catalytic performance of 15% Ni/Al_2O_3 in DRM reaction at 873 ^oC was improved.

In a study by Huynh [17], several HT-derived bimetallic Ni-Fe catalysts with different Fe/Ni ratio (ranging from 0 to 1) were tested in a DRM reaction. It was observed that the catalyst with Fe/Ni ratio of 0.1 exhibited the greatest catalytic activity for 18 h time on stream (TOS). It was reported that the catalyst possessed smaller crystallite size, higher basicity, and enhanced reducibility. All together contributing to the superior activity of the catalyst.

2.2.4 Hydrotalcites and hydrotalcite-derived materials

Hydrotalcite (HT) was first heard of in 1842 in Sweden when a mineral bearing similarity with talc($(Mg_3Si_4O_{10}(OH)_2$) was discovered. The chemical formular is given as $Mg_6Al_2(OH)_{16}CO_3{\cdot}4H_2O$. Its morphology can be compared to that of brucite. In the structure the Mg^{2+} is octahedra and it is linked to 6 OH^- ions at the edges to create infinite sheets whose OH^- ions lies perpendicular to the plane of the layers [25]. Today, hydrotalcites or layered double hydroxides (LDH) is generally referred to a huge group of materials (both natural and

synthetic) with the general formular $[M_{1-x}^{2+}\ M_x^{3+}(OH)_2]$ $[(A_{x/n}{}^{n-}).\ mH_2O]$, where M^{2+} and M^{3+} is the divalent and trivalent ions respectively, x is the mole fraction of the trivalent cation (x = M^{3+}/ (M^{2+} + M^{3+}). Most researchers reported that to obtain a pure hydrotalcite, the value of x must be in the range 0.2-0.33. However, hydrotalcite has been successfully synthesize with x ranging from 0.1-0.5 [26].

Looking at the general formular of LDH, two main components are seen. $[M_{1-x}^{2+}\ M_x^{3+}(OH)_2]$ which indicates the brucite-like layers and $[(A_{x/n}{}^{n-}).\ mH2O]$ which describes the interlayer composition. Most importantly, the Mg^{2+} and Al^{3+} ions in the hydrotalcite structure can be replaced by ions that have similar ionic radii. The ionic radii of Mg^{2+} and Al^{3+} are 0.072 nm and 0.054 nm respectively. For this work, Ni^{2+}(0.069 nm) and Fe^{3+}(0.055 nm) are selected to replace them [27].

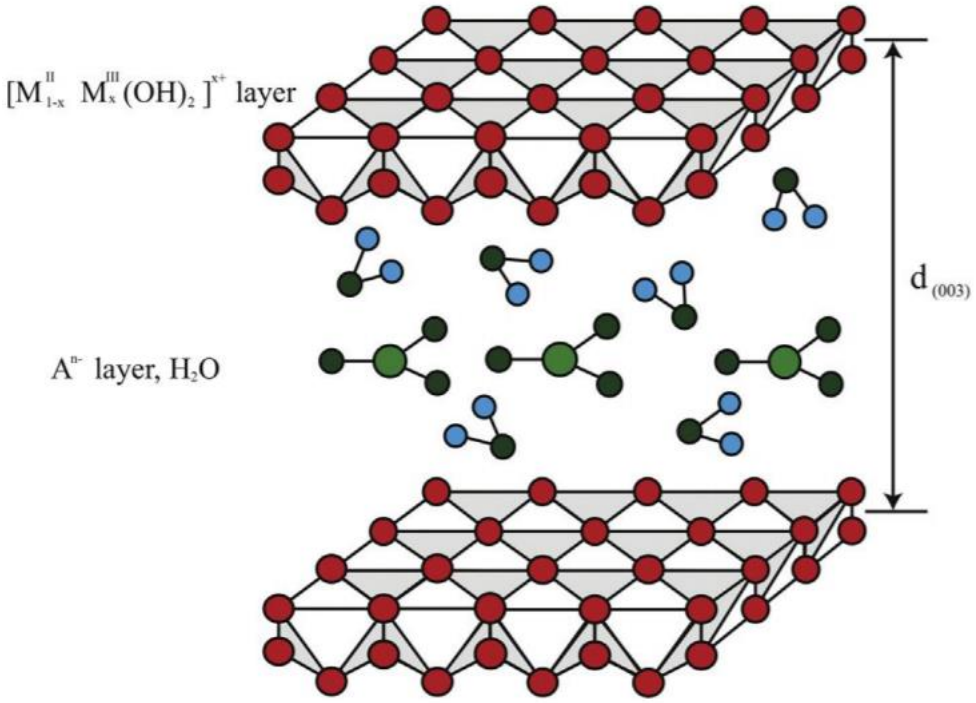

Figure 2.1 Schematic representation of the hydrotalcite structure [28]

Bhattacharyya et al. [29] as one of the first, tested hydrotalcite-derived Ni/Al and Ni/Mg/Al mixed oxides catalysts in the combined dry/steam reforming reactions and compared their catalytic activity to the commercial NiO supported catalysts. Their studies showed that both Ni/Al and Ni/Mg/Al catalysts exhibit very good activity at the similar level to the commercial material.

After them, several researchers have taken interest in this material and have conducted research by checking the activity of HT derived catalyst using different synthesis method, molar ratio, calcination, and nickel loading. Most of them reported that the performance of the HT derived catalyst was dependent on the Mg/Al molar ratio. This ratio was directly proportional to the performance, and the highest Mg loading exhibited highest resistance to coke formation.

2.3 Catalyst Synthesis

Catalyst synthesis is the process of designing a catalyst to optimize catalytic activity, selectivity, stability, and cost. Catalyst synthesis is a systematic approach which includes preparation, aging, filtration, calcination, reduction etc. Many successful catalysts have been synthesized by researchers using methods such as sol-gel technique, anion exchange, induced hydrolysis, urea reduction, microwave or ultrasound treatment, coprecipitation (at high and low supersaturation) [30]. However, the coprecipitation method is one of the most widely used technique for the synthesis of LDH.

2.3.1 Co-precipitation method

Co-precipitation is the most commonly used method of HT preparation. It is a single step method which involves the simultaneous precipitation of substances from a solution by adding a base to a solution containing di and tri-valent cation mixture. One disadvantage to this technique is that the anion which is integrated in the layered double hydroxide should not result in the formation of insoluble salts [31]. It takes place at a either a constant pH or variable pH.

The constant pH technique involves the simultaneous mixture of both the metal salts and the base at a rate that produces a constant pH. On the other hand, the variable pH method involves the formation of metal hydroxides first and further addition of base to cause the co-precipitation. The pH must be chosen in such a way that it is greater enough to produce LDH but lower to prevent the precipitation of a complete divalent metal hydroxide. In the formation of LDH, the pH of the solution must be between pH 7-10 [32]. The constant pH method can result in the formation of crystallites with large size. This can be prevented by the addition of metal salts to base solution under robust stirring [17].

Different coprecipitation methods have been researched namely, co-precipitation at low supersaturation and co-precipitation at high supersaturation. While the former involves a slow or dropwise addition of the cationic solution, the cationic solution in the latter is added at a fast

pace usually using a syringe. For the purpose of this work, co-precipitation at high supersaturation is used.

2.3.2 Aging

The aging process involves a vigorous stirring of the solution at a specific temperature for a given time interval. This stirring is accompanied by the constant supply of nitrogen into the sample. The aging stage of catalyst synthesis helps in the improvement of crystal growth. Through the Oswald ripening mechanism, a dissolution and accumulation of smaller particles into bigger ones occur [33].

Temperature affects both the shape and size of the catalyst. Increasing the aging temperature (from 50 to 90 ^{o}C) results in the formation of larger crystals and a more regular hexagonal shaped catalyst [34].

2.3.3 Calcination

Calcination is a further heat-treatment beyond drying. It is most often the final step in the fabrication of oxide catalyst whereby the catalysts are heated in the presence of oxygen or synthetic air under well-defined conditions. It helps to achieve the desired form for the final catalyst by thermal decomposition and evaporation of components such as hydroxides, nitrates, or carbonates in the catalyst precursor [35]. Several processes occur during calcination. They include loss of chemically bound water or CO_2, changes in pore size distribution, active phase generation, surface conditioning and stabilization of mechanical properties [36].

During the thermo-chemical decomposition of LDH, a sequence of processes take place which involves dehydration, dehydroxylation and loss of interlayer carbonate. These processes occur at different temperature ranges [37].

a) Below 200 ^{o}C – Volatilization of adsorbed and interlayer water molecules;

b) 200 ^{o}C – 500 ^{o}C – Decomposition of interlayer carbonate and hydroxyl groups of the lamellae;

c) Above 500 ^{o}C – Destruction of brucite-like structure and formation of mixed spinel oxide.

It has been concluded by several studies that calcination at high temperatures causes significant reduction in the initial weight of the catalyst (approximately 40%). This occurs because of the

destruction of hydroxide and other materials. This also leads to an increase in the porosity and surface area of the catalyst [38, 39].

2.3.4 Reduction

Reduction is a chemical procedure aimed at converting metal oxides and/or catalyst precursor salts to the active metal by treatment in hydrogen or other reducing agents such as carbon monoxide (CO), synthesis gas (CO and H_2) and hydrazine. The reduction process leads to the formation of high porous materials with very high mechanical strength. [40]

The most vital parameter in the reduction process is temperature. It affects the surface area, extent of reduction, dispersion and metal loading for a given metal-support system. An increase in metal loading usually leads to a decrease in the rate of reduction of a catalyst [41].

2.4 Catalyst Characterization

2.4.1 X-Ray Diffraction (XRD)

X-ray diffraction is a powerful non-destructive technique which is widely used in the determination of bulk structure and composition of heterogeneous catalysts with crystalline structures [42]. Each sample is made up of different components which exhibit their own distinctive diffraction patterns depending on the different planes and angles within every structure. These patterns are used to determine the structure of the sample.

X-ray waves and secondary spherical waves are reflected by atoms when a monochromatic beam of x-rays is allowed to incident on a powder sample. To identify the specific lattice planes that produce peaks at their respective angular position 2Θ, the Bragg's law (Eq. 2.1) is used.

$$\lambda = 2 \times d \times \sin(\Theta) \qquad (2.1)$$

where,

λ = wavelength of the x-rays

d = spacing between crystal lattice planes of atoms

Θ = the angle of incidence

XRD can also be used to estimate the crystallite size. This can be calculated by the peak broadening of the diffraction peaks using the Scherrer equation:

$$d = K\lambda/\beta\cos(\Theta) \qquad (2.2)$$

where,

d = crystallite size

β = full width at half of the maximum intensity of the refection peaks

K = Scherrer constant (Crystallite shape factor)

2.4.2 Nitrogen Adsorption-desorption

Gas adsorption-desorption presents itself as the most common procedure for determining the surface area of porous materials. Basically, there are two main types of adsorption: physisorption and chemisorption. The former is best suited for the measurement of the surface area owing to its low heat of adsorption unaccompanied by any structural changes to the surface during measurement. In the procedure, inert gas is first purged to the samples placed in a glass cell while heating. Liquid nitrogen at 77 K is then used to cool the samples. While increasing the partial pressure of the liquid nitrogen gradually, the amount of N_2 adsorbed at each incremental pressure is recorded. This same process is done for the reverse, where the partial pressure of nitrogen is decreased gradually. The relationship between the volume adsorbed at a particular partial and the volume adsorbed at monolayer coverage is described by the Branauer-Emmett-Teller (BET) equation.

The BET theory is the most used method for the measurement of the internal or specific surface area of porous materials. In principle, BET is a multi-layered adsorption as an extension to the Langmuir adsorption isotherm. There are several assumptions made for this theory including

- Multilayer adsorption
- First layer refers to Langmuir adsorption
- Second layer and further layers refer to condensation of gas into liquid
- The heat of adsorption of the first layer is greater than the heat of condensation of the second layer

Based on these assumptions, the BET equation is given by:

$$\mathbf{1/V(P/P_0-1) = 1/V_mC + (C-1/V_mC)\ (P/P_0)} \qquad \mathbf{(2.3)}$$

Where,

P = Partial pressure of nitrogen

P_0 = saturation pressure at the experimental temperature (vapour pressure of liquid nitrogen)

V = Total volume adsorbed at P

V_m = Volume adsorbed at monolayer coverage

C = Constant

Determination of the BET surface area starts by plotting a graph of P/V(Po-P) against P/Po. This graph yields a straight line in the P/Po range of 0.05 and 0.3 with a slope C-1/V_mC and intercept 1/V_mC. By using these two points on the graph, V_m can be evaluated and the specific surface area can be calculated from that.

The pore size distribution of meso-porous and macro-porous materials can be determined by employing the Banett, Joyner, and Halenda (BJH) method. This method involves using a modification of Kelvin equation and gas desorption isotherm. the measure of adsorbate eliminated from the pores when the relative pressure is reduced is identified with the size of the pores [43].

The International Union of Pure and Applied Chemistry (IUPAC) has grouped sorption isotherms into six types from type I to type VI. The figure below shows the different types of isotherm [44].

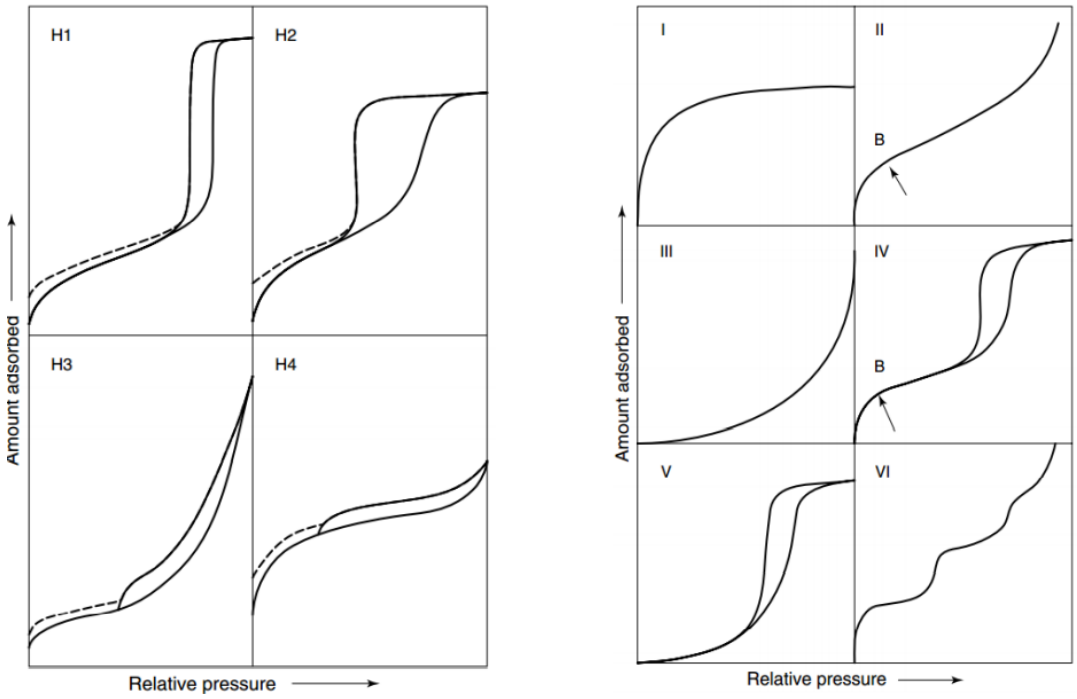

Figure 2.2 Types of physisorption isotherms

The type IV isotherm which is a characteristic for a mesoporous structure (pore size between 2 nm to 50 nm) has a unique hysteresis loop with limiting uptake when the relative pressure increases to high values. These loops exist in different shapes, with each shape identifying a specific pore structure.

2.4.3 Temperature Programmed Reduction (TPR)

Temperature programmed reduction (TPR) is an analytical method that is used to examine the reduction profile of metal oxides, mixed metal oxides under increasing temperatures. It helps to determine the efficient reduction conditions of a catalyst.

In a typical TPR experiment, a reducing gas mixture (3-17% hydrogen in argon or nitrogen) is pumped into the chamber and flows over the sample as the temperature is increased gradually with time. This linear heating allows reduction to be plotted against temperature or time. When the gas reacts with the metal oxide (MO), the resulting products are water and the metal (M), and this reduces the concentration of hydrogen in the gas mixture (Eq. 2.4).

$$\mathbf{MO_n + nH_2 = M + nH_2O} \qquad \mathbf{(2.4)}$$

A thermal conductivity detector (TCD) at the outlet analyses continually the difference in the thermal conductivity of the gas mixture. TPR method also give valuable information about the reproducibility of the catalyst.

2.4.4 Temperature Programmed Desorption (TPD)

Temperature programmed desorption (TPD) is a technique in the field of catalysis which allows the evaluation of the total number of active sites of a catalyst. It is a method used to define the basicity of a catalyst.

During the TPD analysis, a small amount of catalyst sample is placed in a reactor. Helium, argon, or nitrogen at atmospheric pressure is mostly made to flow over the sample. After pre-treatment to produce a reduced sample, an adsorbate gas is injected to the sample under well-defined conditions. The excess gas is removed from the surface at a high linear heating rate and the changes in the pressure of the desorbing gas with time is observed frequently. A TCD detector measures the change in the inert gas stream. If diffusion and readsorption are not limiting, the rate at which species are desorbed from the sample is proportional to the detector response.

2.4.5 Gas Chromatography (GC)

Gas chromatography is an analytical technique used to separate volatile or gaseous compounds. It provides an easy, fast, and simple method to analyse the composition of materials precisely. Gas chromatography involves a sample being vapourised and injected onto the head of a chromatographic column. Samples are divided into two phases; a stationary phase and a mobile phase based on their solubility or affinity for each of the phases. The mobile phase flows over or through the stationary phase. Samples with greater affinity takes more time to pass through the system.

The whole process of the chromatographic analysis can be grouped into 4 main steps: sample collection, sample injection, sample separation, and sample detection. A sample is introduced into a carrier gas stream using an injector and then moves through a column or series of columns where physical separation of the sample takes place. The columns contain a liquid stationary phase which is adsorbed onto the surface of an inert solid. Once the gases pass through the columns, a detector placed at the end of the column records and quantify each component. The different components are recorded as a series of peaks and the area under each of these peaks corresponds to a unique concentration of that component in the original sample.

Quantitative analysis is done by using one of the following methods: area normalization, area normalization with response factor, external standard, internal standard, and standard addition [45]. The external standard is the most widely used method employed to analyse gas. One factor that plays a vital role in the measurement of the outlet gas concentration is the response factor. It is defined as the ratio of the known concentration of the compound being analysed to the response of the detector of that compound.

Response factor = Concentration of known compound / response at the detector

Amount or concentration of components = Response factor × area or peak of component

3 EXPERIMENTAL

3.1 Materials and Equipment

Table 3.1 summarizes all the chemicals and gases used in this work. All were used in their original state without any further purification.

Table 3.1 Summary of chemicals and gases used

No	Materials	Chemical Formula	Manufacturer	Molecular weight (g/mol)	Purity (%)
1	Nickel(II)Nitrate Hexahydrate	$Ni(NO_3)_2.6H_2O$	EMSURE	290.81	≥99
2	Iron(III)Nitrate Nonahydrate	$Fe(NO_3)_3.9H_2O$	EMSURE	403.95	≥99
3	Magnesium Nitrate Hexahydrate	$Mg(NO_3)_2.6H_2O$	EMSURE	256.41	≥99
4	Aluminium Nitrate Nonahydrate	$Al(NO_3)_3.9H_2O$	EMSURE	375.13	≥98.5
5	Sodium Hydroxide	NaOH	EMSURE	40.00	≥99.2
6	Sodium Carbonate	Na_2CO_3	EMSURE	105.99	≥99.9
7	Methane	CH_4	Yara Praxair	16.00	≥99.999
8	Carbon Dioxide	CO_2	Yara Praxair	44.00	≥99.999
9	Helium	He	Nippon gases	2.00	≥99.999
10	Hydrogen	H_2	Nippon gases	2.00	≥99.999
11	Nitrogen	N_2	Yara Praxair	28.00	≥99.999
12	Synthetic air	N_2, O_2	Yara Praxair	28.90	≥99.999

3.2 Catalyst Synthesis

The synthesis method used in this work is co-precipitation at high supersaturation by fast injection. The precursors were made up of nickel, iron, aluminium, and magnesium ions. Each of the catalyst is represented by the general formula CAT-x, where x denotes the molar ratio of Fe to Ni present in the catalyst after reduction. The values of x were obtained by keeping the weight fraction of nickel constant at 20 wt.% while varying that of iron. To obtain a pure HT, the mole fraction of the trivalent cations must be between 0.2 and 0.33. In this study, an average value of 0.25 was used. Therefore, a constant value of 3 was denoted for the atomic ratio of the divalent and trivalent ions. Table 3.2 below shows a summary of the composition of the as prepared catalyst.

Table 3.2 As-prepared catalysts and their compositions

Catalysts	Fe/Ni ratio	Nominal catalyst composition (wt.%)
CAT-0.05	0.05	20Ni – 1Fe - 52MgO – 27Al_2O_3
CAT-0.1	0.1	20Ni – 2Fe - 52MgO – 26Al_2O_3
CAT-0.15	0.15	20Ni – 3Fe - 52MgO – 25Al_2O_3
CAT-0.2	0.2	20Ni – 4Fe - 52MgO – 24Al_2O_3
CAT-0.3	0.3	20Ni – 6Fe - 52MgO – 23Al_2O_3

3.2.1 Coprecipitation at high supersaturation

Based on a modification of the work of Tathod and Gazit [46], five catalyst were prepared using the coprecipitation with high supersaturation method. The mass of the metal nitrates required to prepared 1M solution was weighed into a first beaker. 100 ml of deionized water was added to the metal salts and with the aid of a magnetic bar, the mixture was stirred vigorously. The base solution was also prepared by weighing the respective mass of NaOH and Na_2CO_3 into another beaker and adding 500 ml of deionized water. Under vigorous stirring, the metal nitrate solution was carefully injected into the base solution with the help of a syringe. The slurry was subsequently aged at 85 ^oC under continuous nitrogen purge for 18 h while stirring strenuously. After this process, the resulting mixture then cooled and went through a filtration stage using a vacuum pump. Deionized water was used to wash the mixture to achieve a pH of approximately

7 or neutral. The filter cake obtained after this step was dried in oven at 90 ^{o}C overnight. It was then crushed, sieved, and kept in a desiccator.

The as prepared catalyst precursors were calcined using quartz reactor with flowing synthetic air at 600 ^{o}C for 6 h. The temperature ramp of 5 ^{o}C/min was used.

3.3 Catalyst Characterization

3.3.1 X-Ray Diffraction (XRD)

The x-ray diffraction analysis of the hydrotalcite catalyst (as prepared, calcined, reduced and spent samples) were performed using Bruker-AXS Micro diffractometer D8 Advance with CuKα source of radiation. With a step interval of 1 ^{o}/min, a 2Ɵ range patterns were recorded from 10^{o}-90^{o}.

3.3.2 Nitrogen adsorption-desorption

The nitrogen adsorption-desorption of the as prepared and calcined catalysts were performed using Micromeritics Tristar 3000 unit using liquid nitrogen at -196 ^{o}C. The experiments were conducted by measuring approximately 120 mg of the samples in a tube. Before beginning the experiment, the samples were degassed at 150 ^{o}C overnight under vacuum condition.

3.3.3 Temperature Programmed Reduction (TPR)

The temperature programmed reduction (TPR) profile of the calcined catalyst were performed using The Micromeritics Autochem II ASAP 2920 analyzer. Initially about 100 mg of the calcined samples were measured and placed in a U-shaped quartz reactor on top of a quartz wool layer. The samples then underwent degassing at 200 ^{o}C in helium flow to remove any adsorbed water and carbon dioxide. A reducing gas mixture comprising of 10% hydrogen in argon was purged to the cooled samples at 50 ml/min. Ramping at a rate of 10 ^{o}C/min, the samples were heated to 950 ^{o}C and remained constant at this temperature for 30 minutes.

3.3.4 Temperature Programmed Desorption (TPD)

TPD started immediately after TPR experiments were completed since the same equipment (Micromeritics Autochem II ASAP 2920) was used. The reduced samples (from TPR) were degassed at 600 ^{o}C in helium flow for 30 minutes and then cooled to 80 ^{o}C. A mixture containing 6% carbon dioxide in argon was injected into the reactor at a rate of 50 ml/min. At the same ramp rate used during TPR, the samples were heated to 800 ^{o}C.

3.4 Catalytic activity tests

Building a set-up to investigate the catalytic activity of heterogenous catalyst in a laboratory normally involves three sections. The gas delivery system, the reactor with temperature control and analytic sampling device.

The gas delivery system for this experimented was made up of nitrogen, hydrogen, methane, and carbon dioxide gases. The mass flow of these gases was controlled and monitored using a mass flow controller (Alicat).

A high temperature resistance metal alloy (FeCrAl) was heated in an electrical oven at 900 ^{o}C while purging synthetic gas into it. An Eurotherm 3280 regulator was used to control the temperature during this process. This was done to form a protective coating inside the alloy to prevent its elements from disturbing the activity test. The resulting alloy with inner diameter 5 mm was used as the fixed-bed tubular reactor. A thermocouple (type k) was then installed below the catalyst bed. To monitor the pressure in the reactor, a pressure gauge was installed.

The whole process of catalytic activity test involves several steps:

- Preparation of catalyst sample and placement in reactor
- Reduction
- Reaction
- Cooling and catalyst removal

During the preparation step, 50 mg of the calcined catalyst (300-450 nm) was measured and added to 500 mg of silicon carbide powder (46 grit). This addition was done to ensure proper heat transfer and create enough area for contact of reactant gases. Quartz wool was then pushed into the reactor and the sample was subsequently placed on top of it to form the catalyst bed. Reduction was done after this process. In this step, the montage mixer was used to purge 50 vol% H_2/N_2 with a flowrate of 200 ml/min into the reactor with a temperature at a ramp rate of 5 ^{o}C/min. After the desired reduction temperature was achieved (600 ^{o}C), it was left for 2 hours.

Reaction began after this step by purging 100% N_2 at a flowrate of 200 ml/min whiles ramping up to the desired temperature 700 ^{o}C at a ramp rate of 5 ^{o}C/min. This was done to remove all the H_2 gas left in the reactor after reduction was done. A mixture of 20 vol% N_2, 40 vol% CH_4, and 40 vol% CO_2 at 250 ml/min was then purge into the reactor. The reaction was allowed to run for

24 h TOS for each of the five samples. After the best catalyst was identified, the effect of temperature and a long-term activity test were conducted.

For the reaction at different temperatures, the same procedure was followed but after the reduction stage, N_2 was purge into the reactor while ramping up the temperature to either 650 ^oC and 750 ^oC for the respective test. A mixture of 20 vol% N_2, 40 vol% CH_4, and 40 vol% CO_2 at 250 ml/min was then purge into the reactor and both were allowed to run for 24 h TOS as well.

The long-term activity test on the best catalyst was conducted using the same procedure to the reduction stage. After that stage, N_2 was purge into the reactor while ramping up the temperature to 700 ^oC. In this experiment, a gas mixture of 20 vol% N_2, 40 vol% CH_4, and 40 vol% CO_2 at 120 ml/min was purge into the reactor and allowed to run for 50 h TOS.

The gas chromatograph (Agilent 7890B) was used for analysis of the off-gas mixture. To ensure a smooth flow to the GC, a splitter was installed to divide the off-gas flow into two parts. One of them went to the GC while the other went to ventilation. The amount of CH_4 (n_{CH4}), CO_2 (n_{CO2}), CO (n_{CO}), and H_2 (n_{H2}) were analysed in a molecular sieve-packed column with two TCD detectors. From the GC data, the CH_4 and CO_2 conversions (X_{CH4} and X_{CO2} respectively) as well as the H_2/CO ratio were all calculated using the following equations.

$$\mathbf{X_{CH4} = (n^{in}_{CH4} - n^{out}_{CH4})/ n^{in}_{CH4} \times 100\%} \quad \textbf{(3.1)}$$

$$\mathbf{X_{CO2} = (n^{in}_{CO2} - n^{out}_{CO2})/ n^{in}_{CH4} \times 100\%} \quad \textbf{(3.2)}$$

$$\mathbf{H_2/CO = n_{H2}/n_{CO}} \quad \textbf{(3.3)}$$

4 RESULTS AND DISCUSSION

4.1 Characterization of catalyst

4.1.1 X-ray diffraction of as-prepared catalyst

The XRD profile below (Figure 4.1) corresponds to the as-prepared catalysts which were synthesized by co-precipitation at high saturation. These patterns evince the characteristic diffraction peaks of magnesium aluminium hydroxide carbonate hydrotalcite (JCPDS 22-0700). For instance, the sample CAT-0.05 exhibits four sharp and symmetrical diffraction peaks at 2Θ = 11.43°, 22.94°, 60.61° and 61.88° corresponding to the planes (003), (006), (110), (113) respectively. The other three broad peaks at 2Θ = 34.63°, 38.66° and 45.62° relates to the planes (009), (015) and (018) respectively. These results indicated that the as-prepared catalysts were synthesized well without any impurities phases.

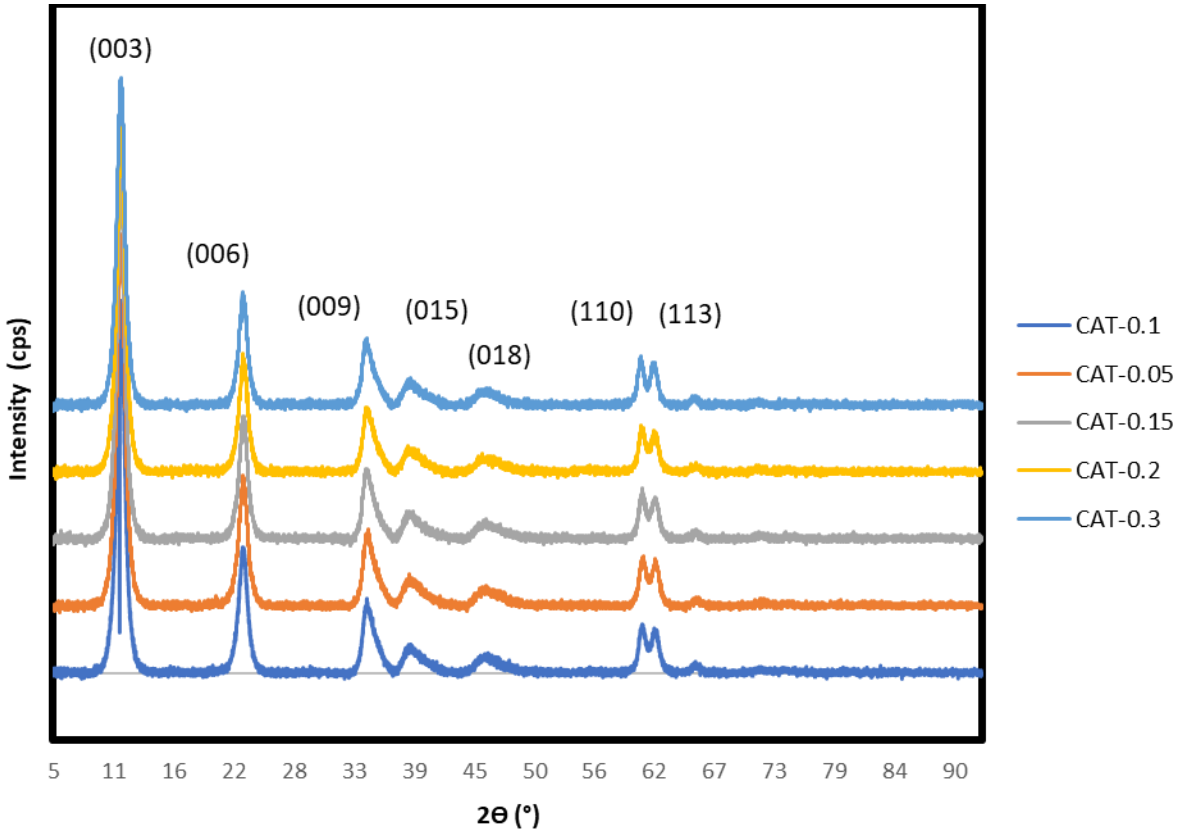

Figure 4.1 X-ray diffraction patterns of as-prepared catalysts

Each diffraction peak has a unique d spacing. To estimate the thickness between a layer comprising of brucite-like sheet and another interlayer, the d-spacing of the (003) diffraction peak was used. Table 4.1 below gives a summary of the values obtained from the calculations. From the table, it can be seen that the thickness increased moderately from 0.774 nm to 0.779

nm as the Fe/Ni ratio in the catalyst increases. However, it should be noted that these values are a little bit smaller than that of magnesium aluminium hydroxide carbonate hydrotalcite (0.784 nm).

Table 4.1 d-spacing of the (003) and (110) reflection planes

Catalyst	$Mg_6Al_2(OH)_{16}CO_3.4H_2O$	CAT-0.05	CAT-0.1	CAT-0.15	CAT-0.2	CAT-0.3
2Θ (°)	11.28	11.43	11.42	11.42	11.42	11.36
d (003) (nm)	0.784	0.774	0.775	0.775	0.775	0.779
2Θ (°)	59.98	60.61	60.59	60.54	60.52	60.42
d (110) (nm)	0.1540	0.1528	0.1528	0.1529	0.1530	0.1532

Again, the average cation-cation distance in the brucite-like layer was found by using the d-spacing of (110) diffraction peak. The same trend was seen in this case with the distance being directly proportional to the Fe/Ni ratio. The values obtained were smaller than that of $Mg_6Al_2(OH)_{16}CO_3.4H_2O$. This could be attributed to the replacement of the Mg^{2+} ion which has a larger ionic radius (0.072 nm) with a smaller Ni^{2+} of ionic radius (0.069 nm) in the lattice.

4.1.2 X-ray diffraction of calcined catalysts

The as-prepared catalysts were calcined at 600 ºC for 6 h. This led to the breakdown of the hydrotalcite-like precursor. This is vividly seen in the XRD patterns where the only visible peaks are that of mixed oxides in Figure 4.2. All the samples presented similar diffraction peaks with their intensities decreasing with an increase in the Fe content.

These diffraction peaks of the calcined catalyst could be associated with the diffraction of NiO (JCDPS01-089-5881) with the peaks at 2Θ = 37.0°, 43.3°, 62.7°, 75.2° and 79.4°. The first sample CAT-0.05 for example showed peaks at 2Θ = 36.2°, 43.3°, 62.9°, 74.8° and 79.5°. These peaks are consistent with previous works on hydrotalcite derived Ni-based catalyst [47, 48]. Due to the possibility of peaks overlap, these peaks could also be linked to either $MgAl_2O_3$, $NiFe_2O_4$, $NiAl_2O_4$ or Fe_2O_3. This makes the phase identification difficult.

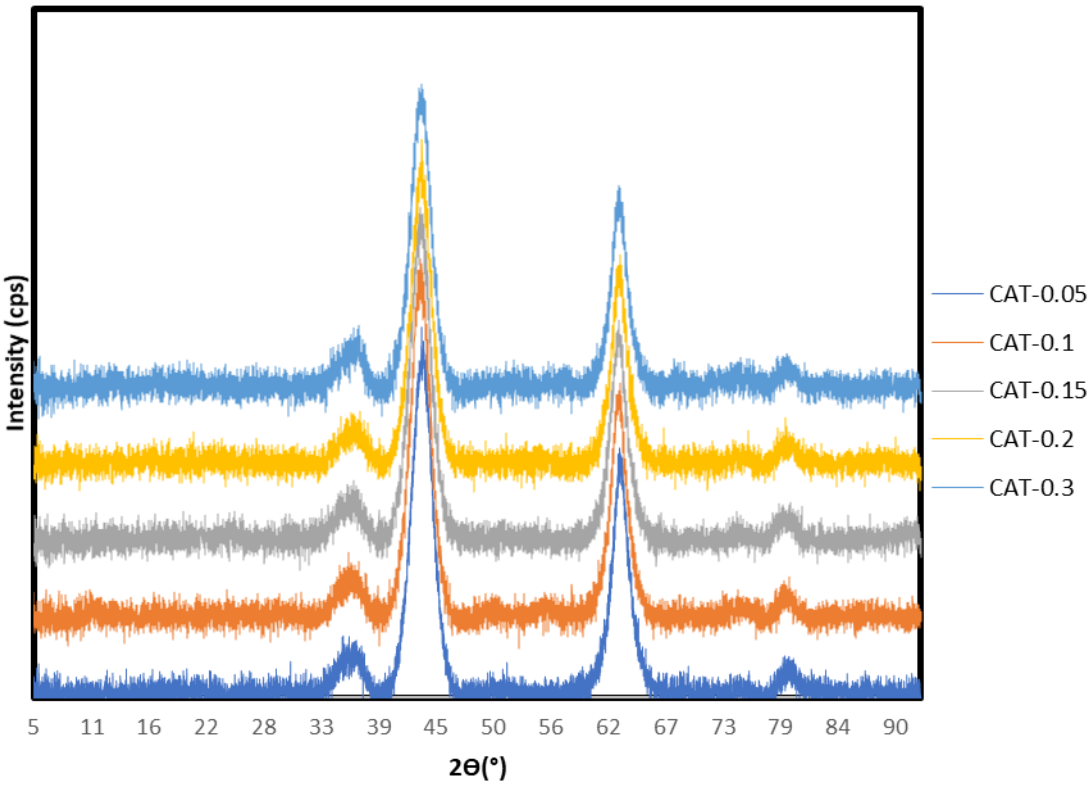

Figure 4.2 X-ray diffraction patterns of calcined catalysts

4.1.3 Nitrogen adsorption-desorption

This experiment was conducted to find the physical properties such as BET surface area, pore size distribution, pore diameter of both the as-prepared precursors and calcined catalysts. Figure 4.3 shows the N_2 adsorption-desorption isotherms of the as-prepared precursors. All the samples showed isotherms which corresponds to the type IV isotherm with hysteresis loop when the range of P/Po is high. From Figure 4.4, the calcined samples recorded similar N_2 adsorption-desorption isotherms as the as-prepared samples. According to the IUPAC classification, these isotherms are unique for mesoporous materials [44].

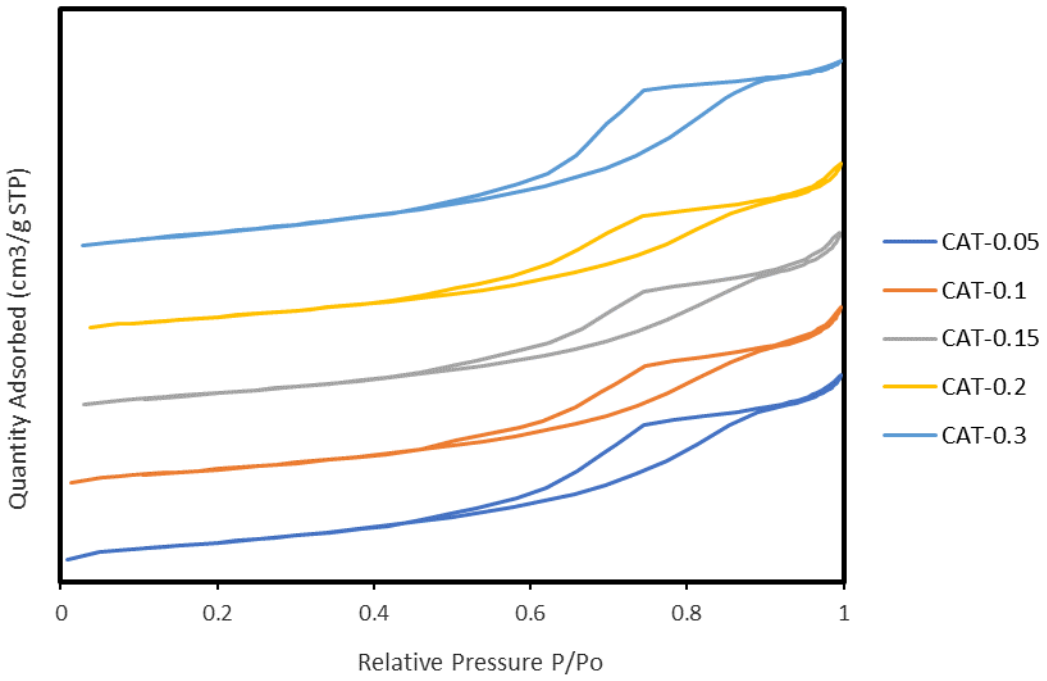

Figure 4.3 Nitrogen adsorption-desorption isotherms of as-prepared catalysts

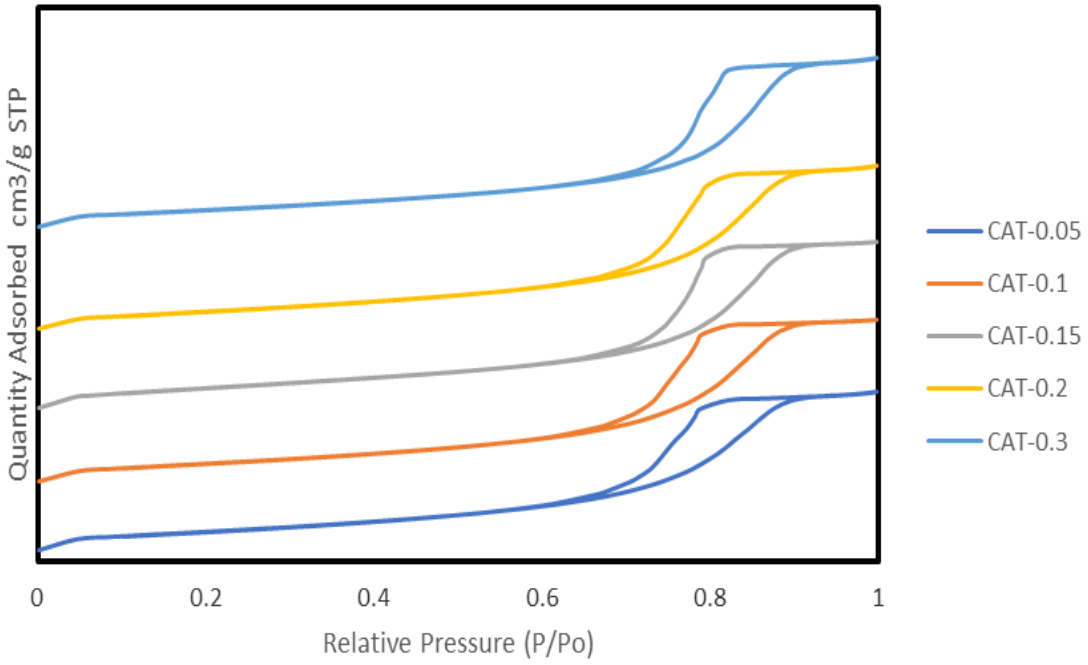

Figure 4.4 Nitrogen adsorption-desorption isotherms of calcined catalysts

Figure 4.5 shows the pore size distribution of the as-prepared samples, while Figure 4.6 presents that of the calcined samples. It is observed that the average pore size increased from 5-10 nm to 7-14 nm due to the thermal decomposition during calcination. Also, these average pore size values further verified that the catalysts were composed of mesoporous materials.

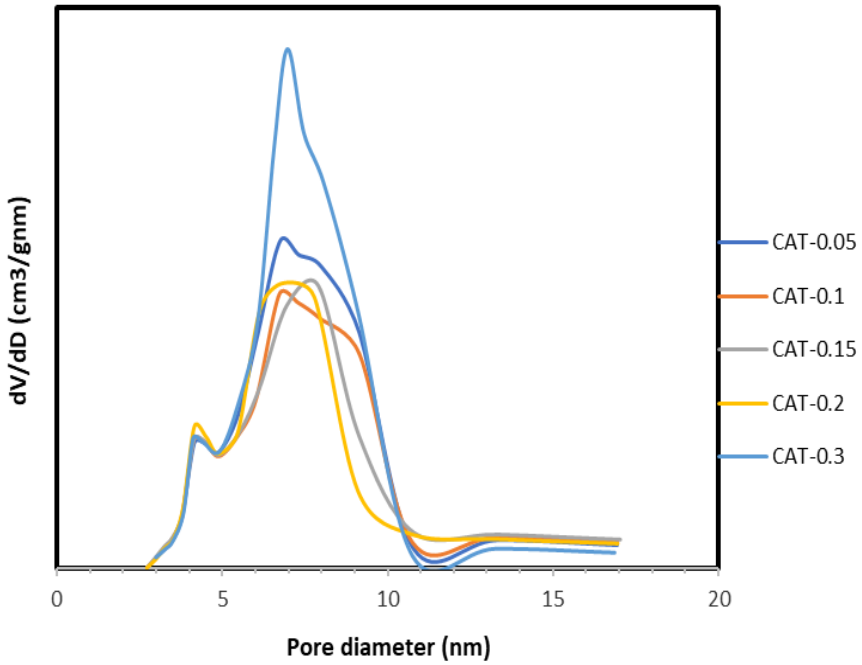

Figure 4.5 Pore size distribution of as-prepared catalysts

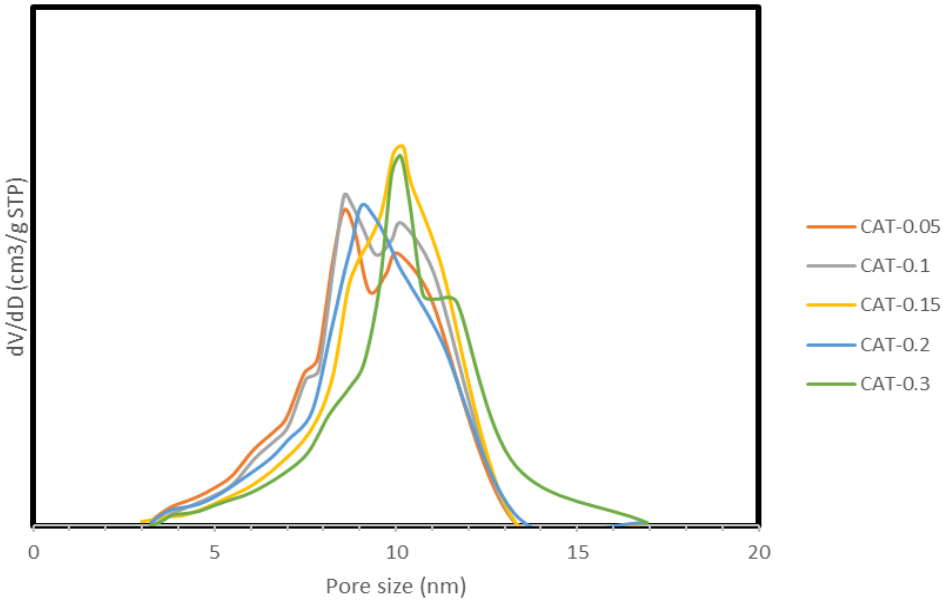

Figure 4.6 Pore size distribution of calcined catalysts

The BET surface area of the as-prepared catalysts was large and generally increased when a Fe is added. When the Fe/Ni ratio increased from 0.2 to 0.3, there was a significant increase in the surface area from 137.86 m^2/g to 166.02 m^2/g.

Table 4.2 Textual properties of the as-prepared and calcined catalyst

Samples	**BET Specific surface area (m^2/g)**		**Pore volume (cm^3/g)**	
	As-prepared	Calcined	As-prepared	Calcined
CAT-0.05	134.69	231.44	0.29	0.62
CAT-0.1	139.64	226.27	0.30	0.62
CAT-0.15	138.66	241.05	0.30	0.64
CAT-0.2	137.86	222.27	0.29	0.64
CAT-0.3	166.02	216.38	0.37	0.65

After calcination, decomposition of the HT-like structure of the catalyst [49] as well as removal of water and other gaseous products occurred. This made it possible for the creation of more pores and channels and led to an increase in the surface area and pore volume of the calcined catalyst compared to that of the as-prepared catalyst.

Based on theoretical calculations, the precursors undergo about 38% reduction in weight after calcination [17]. During the experiment, similar value was achieved for the calcination process of all the samples. The average weight loss was 41.53%. This indicated that the as-prepared samples were successfully calcined. Table 4.3 below gives a summary of the weight of the precursors and calcined samples.

Table 4.3 Comparison between the weight of as-prepared and calcined catalysts

Samples	**Weight of catalyst (g)**		**Percentage reduction (%)**
	As prepared used for calcination	After Calcination	
CAT-0.05	5.00	2.90	42.00
CAT-0.1	5.00	2.93	41.40
CAT-0.15	4.00	2.31	42.25
CAT-0.2	5.00	2.96	40.80
CAT-0.3	5.00	2.94	41.20

4.1.4 Temperature Programmed Reduction (TPR)

The activation of hydrotalcite catalyst was studied during temperature programmed reduction experiment in hydrogen atmosphere. Also, metal-support interaction can be studied using TPR peak temperatures. Higher peak temperature signifies a stronger metal-support interaction. Figure 4.7 presents the H_2 -TPR profiles of the calcined samples.

Generally, the reduction maxima shifted to a low temperature when a small amount of Fe was added. For CAT-0.05, the reduction peak was at 806 ^oC whiles that of CAT-0.3 was at 769 ^oC. A conclusion could be drawn that addition of the Fe promoted or increased the rate of reduction

In most literature, the H_2-TPR profiles show two major reduction peaks for Ni in hydrotalcite catalyst. This is consistent with the results shown in Figure 4.7 below. All the samples showed two significant peaks. While the broad maxima recorded at temperatures ranging from 350 – 450 ^oC could be linked to the reduction of Fe^{3+} to Fe^{2+} [50], the peaks with high intensity could be assigned to either the reduction of Ni^{2+} to Ni or bulk Fe^{3+} and surface Fe^{2+} to Fe [51].

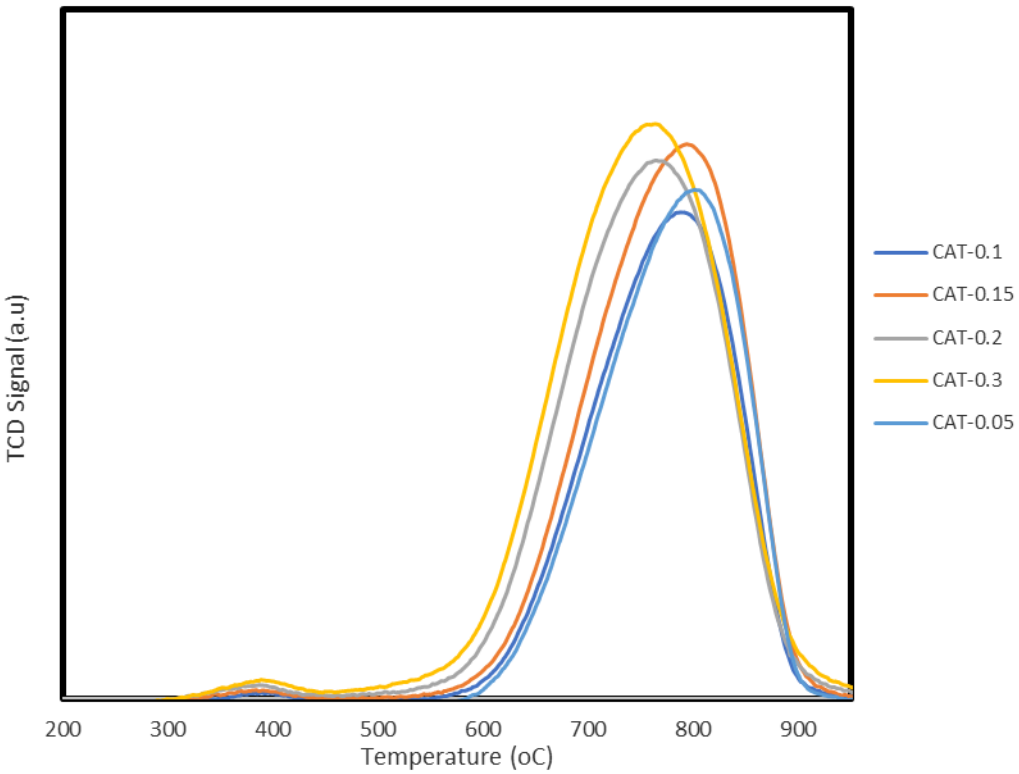

Figure 4.7 TPR patterns of calcined catalysts

4.1.5 Temperature Programmed Desorption (TPD)

To further understand the influence of the composition of each catalyst on their catalytic activity in the DRM reaction, the basic property of all the five samples were studied by temperature programmed desorption. The CO_2-TPD analysis were done right after H_2-TPR analysis of the calcined samples were completed. An assumption is made that prior to CO_2-TPD analysis, all the samples had been reduced in the H_2-TPR experiment.

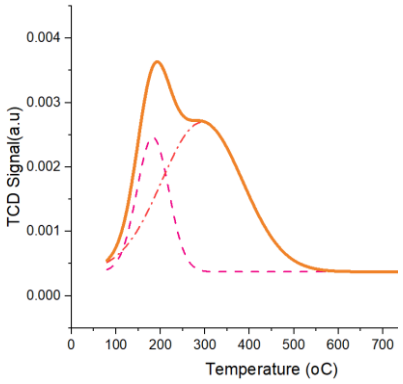

A)

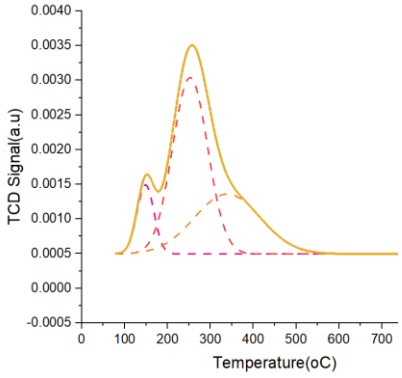

B)

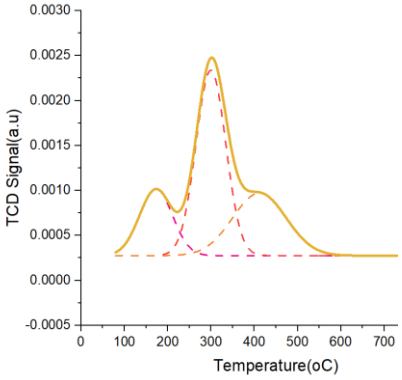

C)

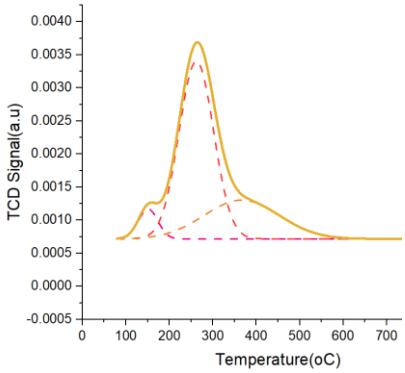

D)

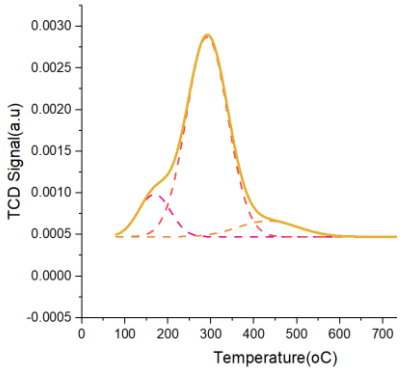

E)

Figure 4.8 TPD patterns (dashed lines = deconvolution) of calcined catalyst A) CAT-0.05 B) CAT-0.1 C) CAT-0.15 D) CAT-0.2 E) CAT-0.3

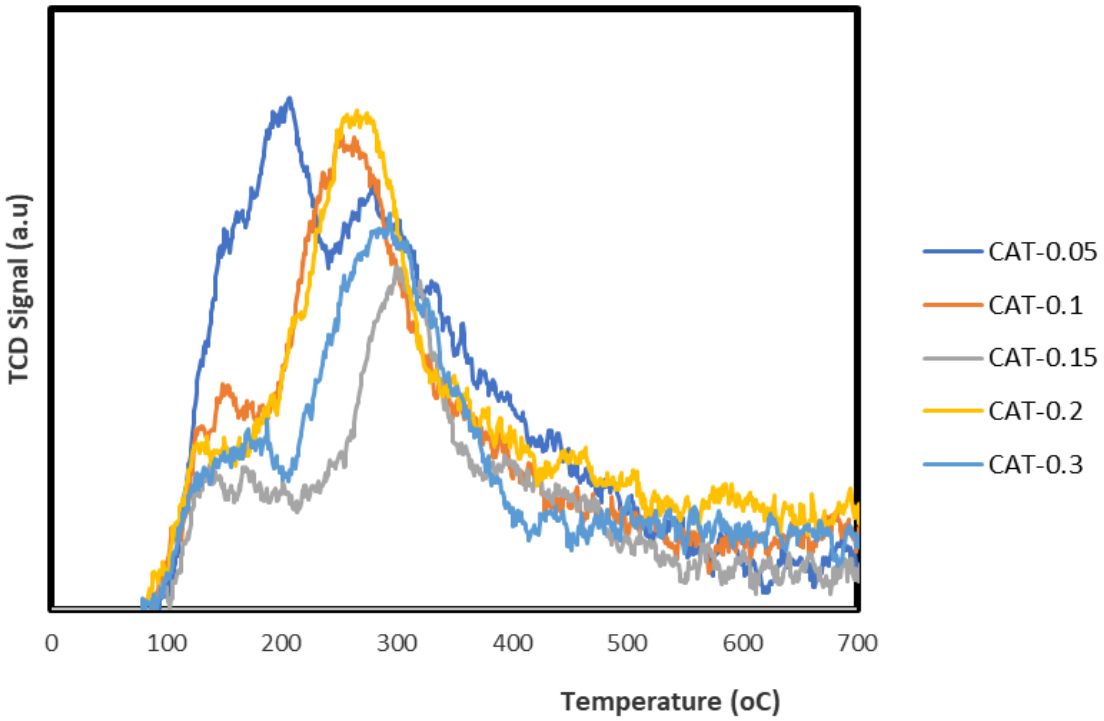

4.9 TPD patterns (without deconvolution) of calcined catalysts

The CO_2-TPD profiles of the calcined materials are presented in Figure 4.8 and 4.9. The Figure 4.9 shows the raw TPD patterns without deconvolution whiles Figure 4.18 is based on Gaussian deconvolution. All the peaks seen in the TPD profiles can be ascribed depending on the temperature at which they are visible. From literature, the basic sites of Mg-Al mixed oxides can be classified according to their different strength as weak (hydroxide group), medium (metal oxygen Lewis pairs) and strong (isolated oxygen anion) [52]. This corresponds to the three CO_2 desorption peaks in the temperature range of 100-500 ^oC [53].

According to Di Cosimo et al [54, 55], the first desorption peak visible at 100-155 ^oC relates to the desorption of CO_2 from weak Bronsted OH^- groups (weak-strength basic sites); the second peak seen at 190-250 ^oC is attributed to the formation of bidentate carbonate (medium-strength basic sites) and lastly the peak at temperatures above 280 ^oC is assigned to the desorption of CO_2 bounded with low coordination oxygen anion(strong basic sites).

Apart from the CAT-0.05 and CAT-0.3 which were predominantly made up of medium basic sites at 74% and 78% respectively, all the remaining catalyst had both the medium and strong basic sites contributing significantly to their basicity. This is clearly seen in the Table 4.4. The CAT-0.05 interestingly did not show any strong basic sites. This means that most of the CO_2 adsorbed to the metallic surface was not due to bonding with low coordination oxygen anion.

Table 4.4 Basicity distribution of reduced catalysts

Samples	Weak sites	Medium sites	Strong sites
CAT-0.05	26%	74%	-
CAT-0.1	10%	55%	35%
CAT-0.15	20%	50%	30%
CAT-0.2	6%	64%	30%
CAT-0.3	13%	78%	9%

4.2 The catalytic performance of Ni-Fe catalysts in DRM reaction

4.2.1 Catalytic activity at 700 ºC

The DRM reactions was conducted at 700 ºC, 1 bar and a total gas flowrate of 250 ml/min corresponding to a GHSV of 300,000 $mLg^{-1}h^{-1}$ in the ratio (N_2: CH_4: CO_2= 20:40:40). The nitrogen was used as an internal standard as part of the total flow. Since it is inert, the amount of nitrogen at the inlet will be the same at the outlet. This helped to determine the total flow out as well as the flow at the outlet of the individual reactants. In each reaction, a graph of CH_4 conversion, CO_2 conversion and H_2/CO ratio against time was plotted. In general, all the catalyst samples were stable for the time on stream with the exception of CAT-0.1 which started with a highest initial conversion but deactivated quickly with time.

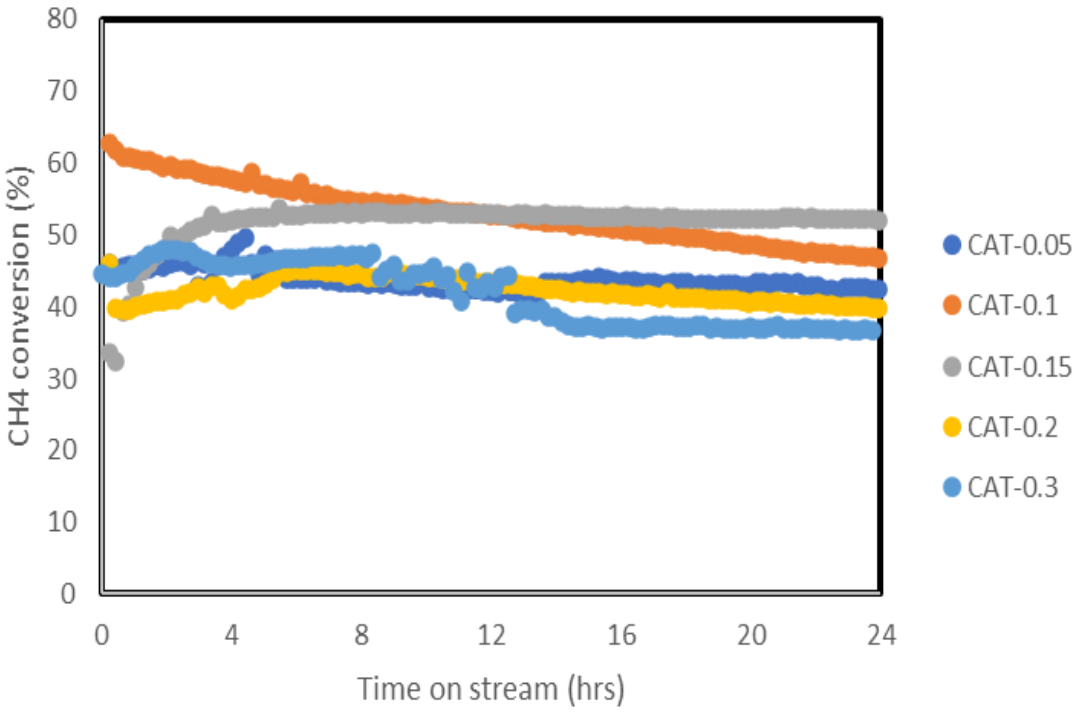

Figure 4.10 CH_4 conversion for the different catalyst at 700 ^oC

Even though most of the samples showed a stable characteristic over the time on stream, each sample presented a unique behaviour during the course of the reaction. The catalytic activity of the samples increased as the Fe/Ni ratio increased from 0.05 to 0.15. This is indicated by their CH_4 and CO_2 conversions in Figure 4.10 and 4.11. The sample CAT-0.1 showed an interesting conversion profile. It had the highest initial conversion (both CH_4 and CO_2) value but gradually decreased to a final CH_4 and CO_2 conversions of 47 and 59% respectively.

A vivid explanation cannot be given at this point since in-situ characterization were not conducted in this work. But this could be attributed to the sintering of catalyst particles. The sample CAT-0.15 presented itself as the best catalyst due to its higher CH_4 and CO_2 conversions compared to the remaining samples. Initially, it had the lowest conversions but gently increased to a final conversion of 52 and 65% respectively. From Figure 4.11, the CO_2 conversion is higher than that of the CH_4 because of the occurrence of the reverse water gas shift reaction (RWGS). This finding is not surprising because from the nitrogen adsorption-desorption experiment, the BET surface area of the CAT-0.15 was the highest among all the calcined samples. The catalyst with the Fe/Ni ratio of 0.2 and 0.3 showed the least activities. This might be as a result of an increase in coverage of the Fe over the surface of the Ni.

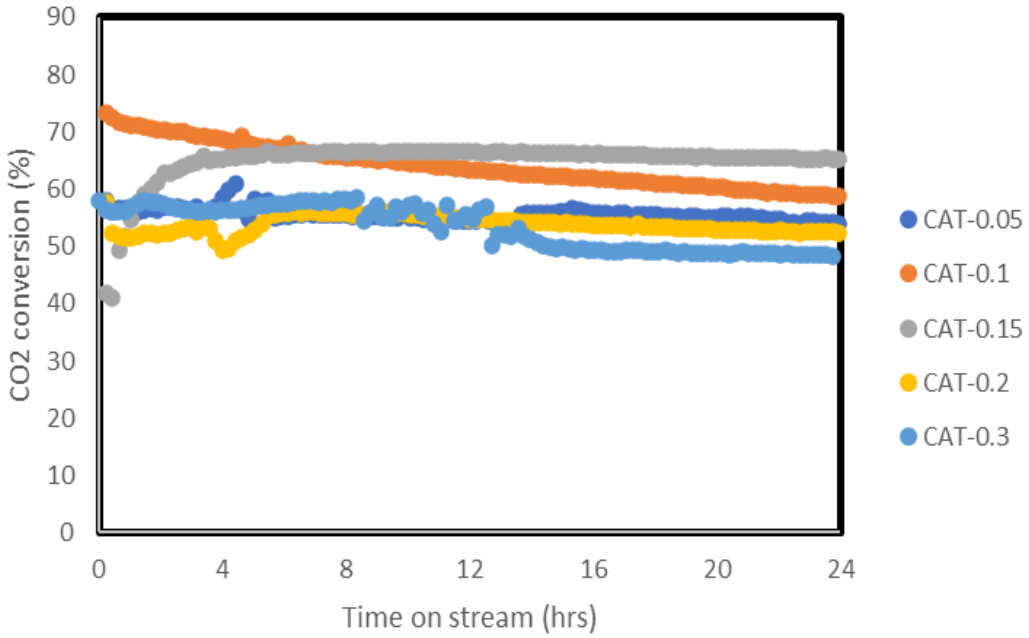

Figure 4.11 CO_2 conversion of different catalyst at 700°C

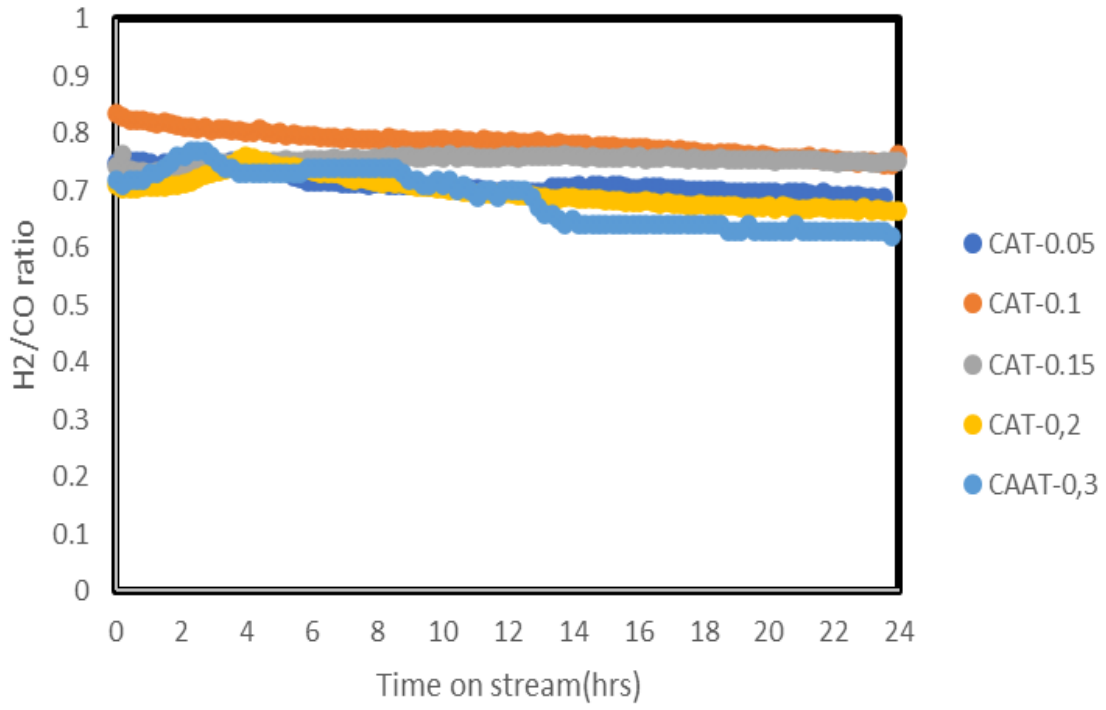

Figure 4.12 H_2/CO ratio of the different catalyst at 700°C

It is suggested by study on bimetallic Fe catalyst that in the process of DRM, Fe dealloys with Ni. This is as result of the Fe been oxidized by the adsorbing CO_2 [56]. The occurrence of this mechanism is possible when Fe is substituted in the HT structure during DRM reaction.

In a bimetallic Ni-Fe catalyst, the amount of nickel in the alloy related to the activity and stability of the catalyst. When the amount of Fe in the catalyst is increased significantly, the catalyst becomes relatively inactive.

Tsoukalou et al. [57] conducted a study by preparing $LaNi_{0.8}Fe_{0.2}O_3$ perovskite catalysts using co-precipitation method. The study revealed that in a Ni-Fe bimetallic catalyst, the Fe does not only alloy with the Ni but also form a solid solution with La. This encapsulation of Ni by $LaFeO_3$ drastically reduced the activity of the catalyst.

From the stoichiometric point of view, the H_2/CO ratio for the DRM reaction is equal to 1. However, in this study even the best catalyst had a ratio lower than unity. This could be ascribed to the reverse water gas shift (RWGS) side reaction. From Figure 4.12 above, the H_2/CO exhibited the same trend seen in the plots of the conversions. When a small amount of Fe was added to some extent to the catalyst, the ratio increased. For catalyst with Fe/Ni ratio greater than 0.15, the H_2/CO ratio also decreased.

4.2.2 Catalytic activity at different temperatures

The performance of the CAT-0.15 was tested at both 650 ^oC and 750 ^oC with a flow of 250 ml/min. From the thermodynamic perspective, the equilibrium position shifts to the production of more reactant when temperature is reduced and vice versa. Therefore, the test was conducted to study the stability of the catalyst at these temperatures. After reduction for 4 hours using 50 vol% H_2/N_2, 100 vol% N_2 was purged into the reactor to remove all the H_2. Then the tests were conducted at 650 ^oC and 750 ^oC and a total gas flowrate of 250 ml/min corresponding to a GHSV of 300,000 $mLg^{-1}h^{-1}$ in the ratio (N_2:CH_4: CO2 = 20:40:40). At high temperatures, there is the tendency for metal particle sintering which can lead to deactivation. On the other hand, low temperatures can also favour carbon formation. This is showed in Figure 4.13, where at 750 ^oC the catalyst deactivated quickly even though it had the highest CH_4 conversion. Whiles the reaction run at 650 ^oC recorded the lowest CH_4 conversion which could be attributed to carbon formation.

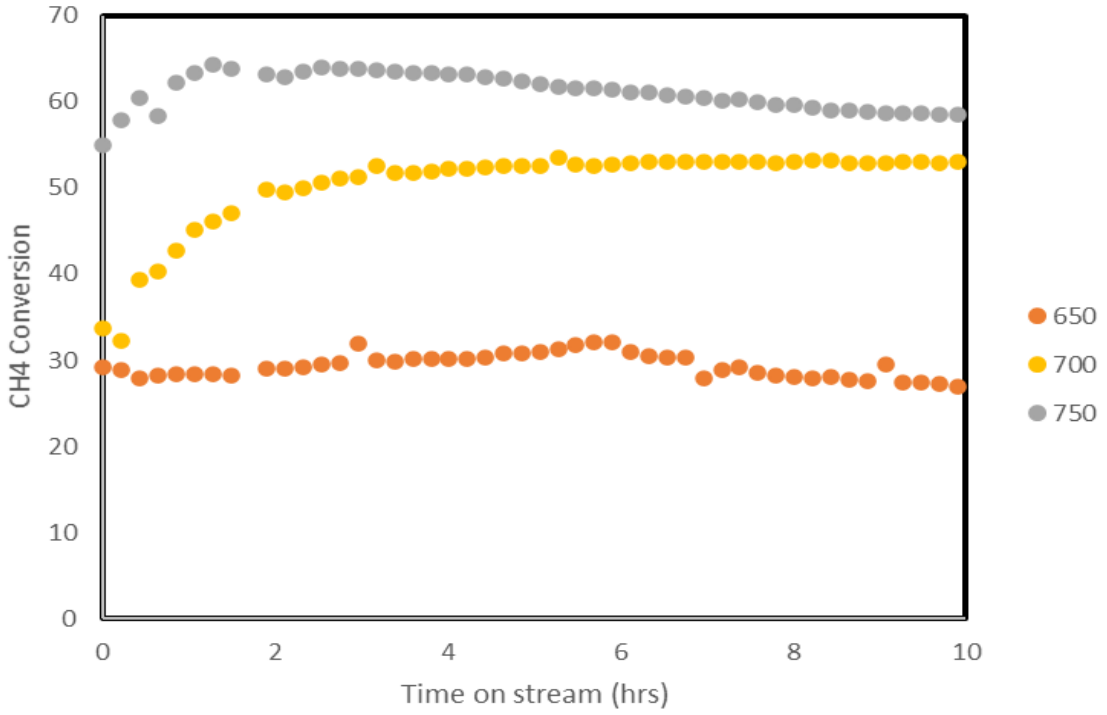

Figure 4.13 CH_4 conversion of CAT-0.15 at different temperatures

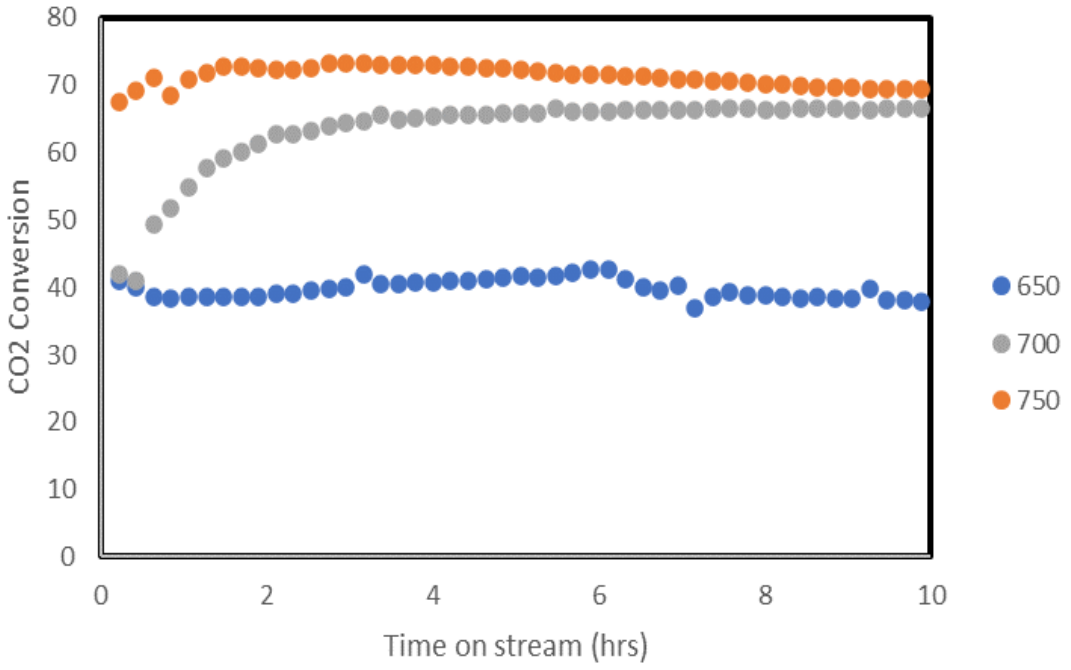

Figure 4.14 CO_2 conversion of CAT-0.15 at different temperatures

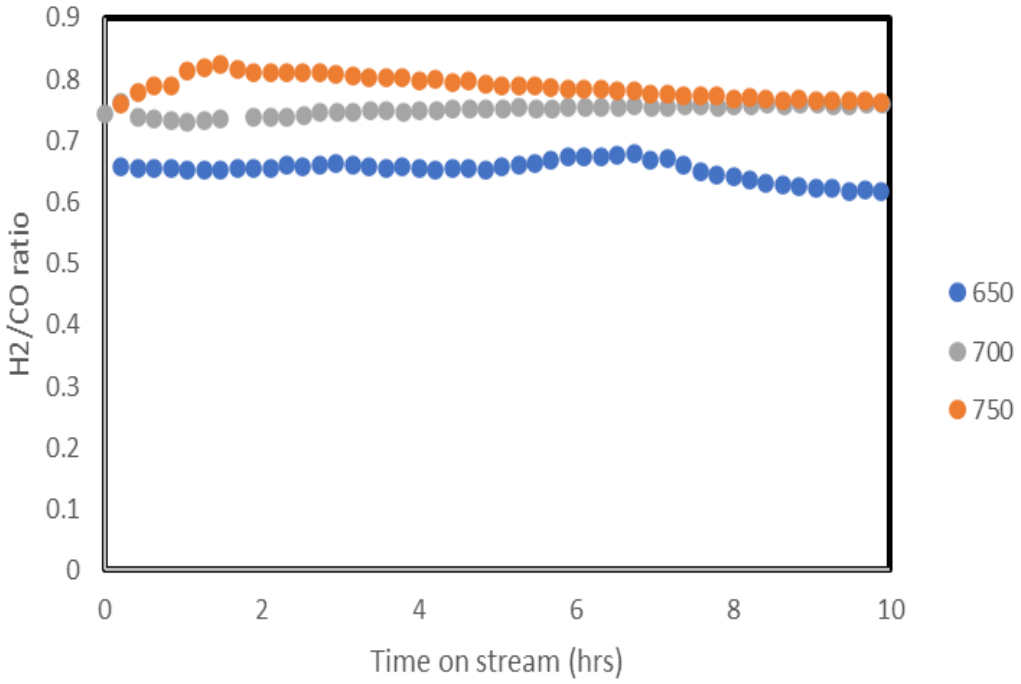

Figure 4.15 H_2/CO ratio of CAT-0.15 at different temperatures

From the plots above, it is revealed that the activity of the catalyst was consistent with thermodynamic principles. Higher activity was achieved when the temperature was increased. After 10 h TOS, the catalyst seemed to deactivate slightly. This could be attributed to the carbon formation or sintering during the process of the reaction.

4.2.3 Long term activity test

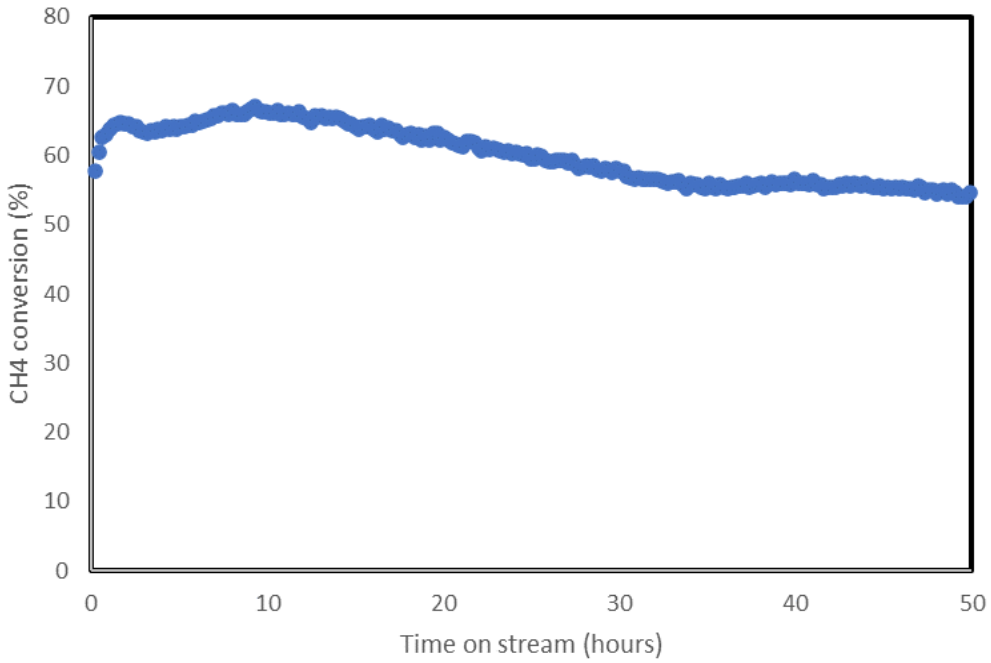

Figure 4.16 CH_4 conversion of CAT-0.15 in long term DRM activity test at 700 ^oC, gas flow of 120 mL/min

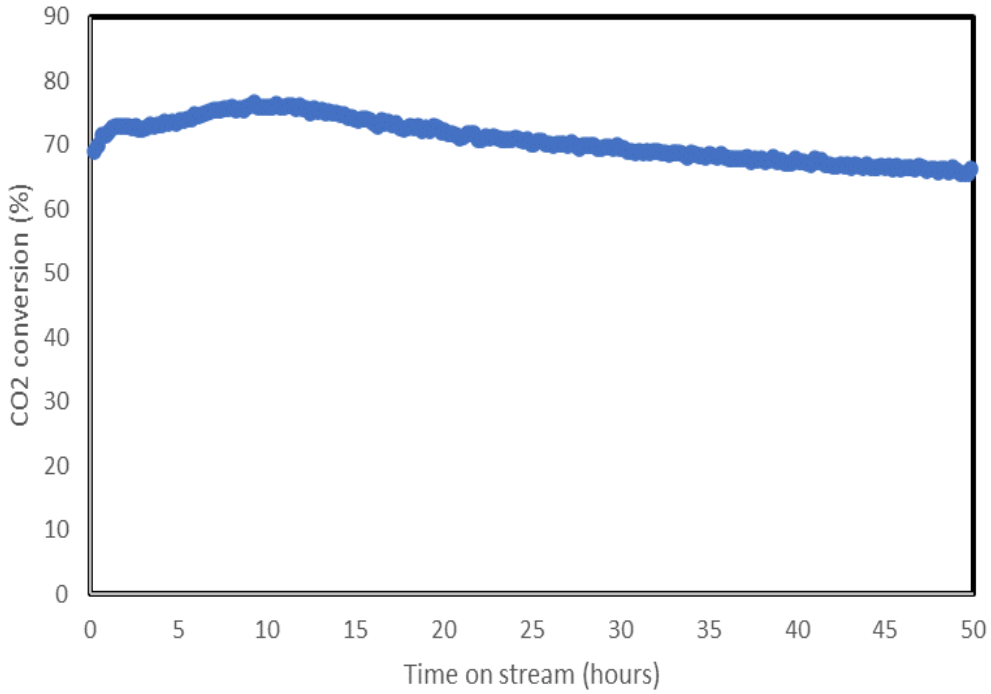

Figure 4.17 CO_2 conversion of CAT-0.15 in long term DRM activity test at 700 ^oC, gas flow of 120 mL/min

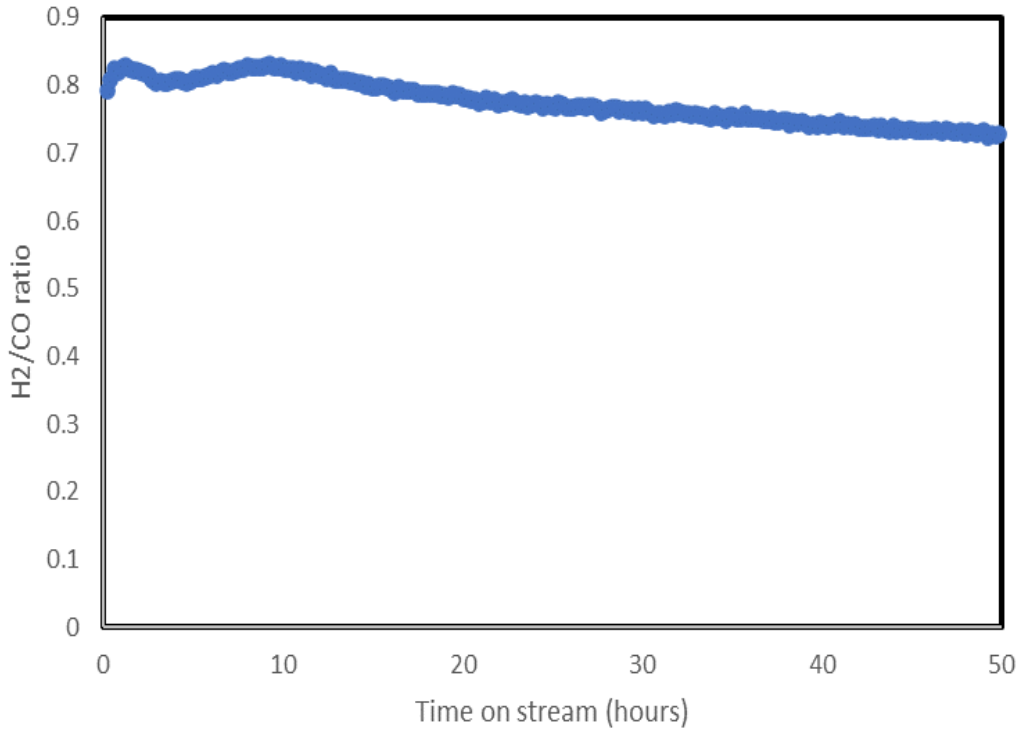

Figure 4.18 H_2/CO ratio of CAT-0.15 in long term DRM activity test at 700 ^oC, gas flow of 120 mL/min

Long test activity test was conducted to check the stability of the catalyst over a long time on stream. For this experiment a lower flowrate of 120 ml/min was used, corresponding to GHSV of 144,000 $mLg^{-1}h^{-1}$. The main reason was to help reduce the increased pressure in the system. In Figure 4.16 and 4.17, catalyst showed a higher initial conversion but increased steadily to a CH_4 and CO_2 conversion of approximately 64% and 74% respectively after 15 h. And started declining gradually and remaining stable at a CH_4 and CO_2 conversion of approximately 55% and 68% after 33 h TOS. In Figure 4.18 the initial H_2/CO was approximately 0.8 but gradually decreased after 13 h TOS to a final H_2/CO of 0.73. Compared to the reaction with a flow rate of 250 ml/min, the reaction at 120 ml/min produce higher final conversions. During the reaction at 120 ml/min, the GHSV is reduced and this could be the reason for the increased in the final conversions.

5 CONCLUSION AND RECOMMENDATION

5.1 Conclusion

This thesis deals with the study of the catalytic activity of different Ni-Fe bimetallic catalysts derived from hydrotalcite materials in a dry reforming of methane reaction. Five different Ni-Fe bimetallic catalyst supported on mixed oxides $MgO\text{-}Al_2O_3$ were synthesized using the co-precipitation at high super saturation method by fast injection.

While the nickel loading was kept constant at 20 wt.%, the Fe/Ni ratio was increased from 0.05 to 0.3 from the analysis conducted such as XRD, TPR, TPD and BET the following can be concluded

- The hydrotalcite precursors were successfully synthesized. Based on the XRD data both the as-prepared and calcined catalyst showed no sign of impurities.
- The catalysts were truly calcined at 600 ^oC for 6 hours. According to the BET results, the calcined catalyst showed larger surface area and pore volume indicating the decomposition of the HT structure. The surface area of the calcined samples was larger than that of the as-prepared catalysts showing the successful decomposition of the hydrotalcite-like structure.
- Upon the addition of small amount of Fe, the reduction peaks were lowered demonstrating the propensity of Fe promoting the reduction of Ni. This was based on the results from TPR experiment.

The DRM reaction was conducted at 700 ^oC with a GHSV of 300,000 $mLg^{-1}h^{-1}$. The activities of all the samples were tested and a conclusion can be made that upon a small increase in the Fe/Ni (less than 0.2), the catalytic activity also increased. However, upon further increase in the ratio (greater than 0.2), relatively lower activities were recorded. The Fe was said not to only form alloy with Ni but could be oxidized by the adsorbing CO_2 to form iron oxide which can cover the surface of the nickel particles.

The CAT-0.15 presented superior conversions and that made it the overall best sample. Interestingly, previous experiments indicated the catalyst with the Fe/Ni ratio of 0.1 to be the best sample[17]. Therefore, a conclusion could be made that the optimum Fe/Ni ratio for this Ni-Fe bimetallic catalyst on mixed $MgO\text{-}Al_2O_3$ support could be in the range of 0.1 to 0.15.

5.2 Recommendation

Based on the promising data of Ni-Fe bimetallic catalyst in the dry reforming of methane reaction, the following recommendations have been put together.

- One of the main challenges that is faced by the industry to commercialize the dry reforming of methane reaction is the coke formation. Coke formation that not only increase the overall cost of the reaction but also plays a major role in the deactivation of the catalysts. A study should be focused on investigating the coke formation mechanisms or other factors that could cause deactivation of the nickel iron hydrotalcite catalysts during the course of the reaction.
- From the catalytic test at different temperatures, it was realised that the catalyst showed higher activity when the temperature was increased. More research can be done to check the conversions and stability of the Ni-Fe at higher temperatures from 750 ^{o}C to 800 ^{o}C.
- Further experiment could be conducted to find the optimum Fe/Ni ratio that will yield the highest activity with the ratio of 0.1 to 0.15.

REFERENCES

[1] P. Agreement, "Paris agreement," in *Report of the Conference of the Parties to the United Nations Framework Convention on Climate Change (21st Session, 2015: Paris). Retrived December*, 2015, vol. 4, p. 2017: HeinOnline.

[2] D. Y. Kalai, K. Stangeland, Y. Jin, and Z. J. J. o. C. U. Yu, "Active and stable hydrotalcite derived Ni catalysts for CO2 reforming of methane: comparison with catalysts by incipient wetness," *Journal of CO2 Utilization*, vol. 25, pp. 346-355, 2018.

[3] N. A. K. Aramouni, J. G. Touma, B. A. Tarboush, J. Zeaiter, and M. N. Ahmad, "Catalyst design for dry reforming of methane: Analysis review," *Renewable and Sustainable Energy Reviews*, vol. 82, pp. 2570-2585, 2018.

[4] Paulina Summa, B. Samojeden, and M. Motak, "<Dry_and_steam_reforming_of_methane_Comparison_and_.pdf>," *Polish Journal of Chemical Technology*, vol. 21, pp. 31-37, 2019.

[5] M. Akri *et al.*, "Atomically dispersed nickel as coke-resistant active sites for methane dry reforming," *Nat Commun*, vol. 10, no. 1, p. 5181, Nov 15 2019.

[6] S. A. Theofanidis, V. V. Galvita, H. Poelman, and G. B. Marin, "Enhanced Carbon-Resistant Dry Reforming Fe-Ni Catalyst: Role of Fe," *ACS Catalysis*, vol. 5, no. 5, pp. 3028-3039, 2015.

[7] R. Dębek, M. Motak, T. Grzybek, M. Galvez, and P. Da Costa, "A Short Review on the Catalytic Activity of Hydrotalcite-Derived Materials for Dry Reforming of Methane," *Catalysts*, vol. 7, no. 12, 2017.

[8] J.-E. Min, Y.-J. Lee, H.-G. Park, C. Zhang, and K.-W. Jun, "Carbon dioxide reforming of methane on Ni–MgO–Al2O3 catalysts prepared by sol–gel method: Effects of Mg/Al ratios," *Journal of Industrial and Engineering Chemistry*, vol. 26, pp. 375-383, 2015.

[9] W.-J. Jang, J.-O. Shim, H.-M. Kim, S.-Y. Yoo, and H.-S. Roh, "A review on dry reforming of methane in aspect of catalytic properties," *Catalysis Today*, vol. 324, pp. 15-26, 2019.

[10] P. Cao, S. Adegbite, H. Zhao, E. Lester, and T. J. A. E. Wu, "Tuning dry reforming of methane for FT syntheses: A thermodynamic approach," *Applied Energy*, vol. 227, pp. 190-197, 2018.

[11] J. R. Rostrup-Nielsen, "Catalytic steam reforming," in *Catalysis*: Springer, 1984, pp. 1-117.

[12] M. K. Nikoo and N. J. F. P. T. Amin, "Thermodynamic analysis of carbon dioxide reforming of methane in view of solid carbon formation," *Fuel Processing Technology*,vol. 92, no. 3, pp. 678-691, 2011.

[13] S. J. N. Helveg, "C. Ló pez-Cartes, J. Sehested, PL Hansen, BS Clausen, JR Rostrup-Nielsen, F. Abild-Pedersen, JK Nørskov," *Nature*, vol. 427, p. 426, 2004.

[14] J. Rostrup-Nielsen and L. J. Christiansen, *Concepts in syngas manufacture*. World Scientific, 2011.

[15] Y. Wang, L. Yao, S. Wang, D. Mao, and C. Hu, "Low-temperature catalytic CO2 dry reforming of methane on Ni-based catalysts: A review," *Fuel Processing Technology*, vol. 169, pp. 199-206, 2018.

[16] P. Djinović, I. G. O. Črnivec, B. Erjavec, and A. J. A. C. B. E. Pintar, "Influence of active metal loading and oxygen mobility on coke-free dry reforming of Ni–Co bimetallic catalysts," *Applied Catalysis B: Environmental*, vol. 125, pp. 259-270, 2012.

[17] H. L. Huynh, "Synthesis, characterization, and activity of bimetallic Ni-Fe hydrotalcite-derived catalysts in dry reforming of methane," University of Stavanger, Norway, 2018.

[18] Y. H. Hu and E. J. C. Ruckenstein, "Catalytic conversion of methane to synthesis gas by partial oxidation and CO2 reforming," *ChemInform*, vol. 35, no. 49, pp. no-no, 2004.

[19] H. Ay and D. Üner, "Dry reforming of methane over CeO2 supported Ni, Co and Ni–Co catalysts," *Applied Catalysis B: Environmental*, vol. 179, pp. 128-138, 2015.

[20] K. Świrk, M. E. Gálvez, M. Motak, T. Grzybek, M. Rønning, and P. J. C. C. Da Costa, "Dry reforming of methane over Zr-and Y-modified Ni/Mg/Al double-layered hydroxides," *Catalysis Communication*,vol. 117, pp. 26-32, 2018.

[21] J. Guo, H. Lou, H. Zhao, D. Chai, and X. Zheng, "Dry reforming of methane over nickel catalysts supported on magnesium aluminate spinels," *Applied Catalysis A: General*, vol. 273, no. 1-2, pp. 75-82, 2004.

[22] J. Ashok, M. Subrahmanyam, and A. J. I. j. o. h. e. Venugopal, "Hydrotalcite structure derived Ni–Cu–Al catalysts for the production of H2 by CH4 decomposition," *International Journal of Hydrogen Energy*, vol. 33, no. 11, pp. 2704-2713, 2008.

[23] J.-H. Kim, D. J. Suh, T.-J. Park, and K.-L. J. A. C. A. G. Kim, "Effect of metal particle size on coking during CO2 reforming of CH4 over Ni–alumina aerogel catalysts," *Applied Catalysis A: General* vol. 197, no. 2, pp. 191-200, 2000.

[24] Z. Song *et al.*, "Improved Effect of Fe on the Stable NiFe/Al2O3 Catalyst in Low-Temperature Dry Reforming of Methane," *Industrial & Engineering Chemistry Research*, vol. 59, no. 39, pp. 17250-17258, 2020.

[25] K. Mette, T. Ressler, and M. Muhler, "Development of hydrotalcite-derived Ni catalysts for the dry reforming of methane at high temperatures," Technische Universität Berlin, 2015.

[26] F. Cavani, F. Trifiro, and A. J. C. t. Vaccari, "Hydrotalcite-type anionic clays: Preparation, properties and applications," *Catalysis Today*, vol. 11, no. 2, pp. 173-301, 1991.

[27] D. R. Lide, "Handbook of chemistry and physics," 1999. CRC Press

[28] R. Salomao, L. Milena, M. Wakamatsu, and V. C. J. C. I. Pandolfelli, "Hydrotalcite synthesis via co-precipitation reactions using MgO and Al (OH) 3 precursors,"*Ceramics International*, vol. 37, no. 8, pp. 3063-3070, 2011.

[29] A. Bhattacharyya, V. W. Chang, and D. J. J. A. c. s. Schumacher, "CO2 reforming of methane to syngas: I: evaluation of hydrotalcite clay-derived catalysts," *Applied clay science*, vol. 13, no. 5-6, pp. 317-328, 1998.

[30] F. Kovanda, E. Jindová, K. Lang, P. Kubát, and Z. J. A. C. S. Sedláková, "Preparation of layered double hydroxides intercalated with organic anions and their application in LDH/poly (butyl methacrylate) nanocomposites," *Applied clay science*, vol. 48, no. 1-2, pp. 260-270, 2010.

[31] A. Parra Camacho, "NiFe hydrotalcite-derived catalyst for CO2 reforming of methane: the impact of calcination and reduction temperature," University of Stavanger, Norway, 2019.

[32] A. Bhattacharyya, "Method of hydrocarbon reforming and catalyst precursor," ed: Google Patents, 2000.

[33] L. Hickey, J. Kloprogge, and R. J. J. o. M. S. Frost, "The effects of various hydrothermal treatments on magnesium-aluminium hydrotalcites," *Journal of Material Science*, vol. 35, no. 17, pp. 4347-4355, 2000.

[34] R. Wang, X. Liang, Y. Peng, X.-w. Fan, and J.-x. Li, "Effect of the reaction temperature on nanocrystallites MgAl2O4 spinel ceramic precursor," in *J. Ceram. Proc. Res*, 2009, vol. 10, pp. 780-782.

[35] C. H. Bartholomew and R. J. Farrauto, *Fundamentals of Industrial Catalytic Processes*. Hoboken, New Jersey: A JOHN WILEY & SONS, INC., PUBLICATION 2006.

[36] J. T. Richardson, *Fundamental and Applied Catalysis- Principles of Catalyst Development*. USA: Springer, 1989.

[37] T. P. F. Teixeira, S. Aquino, S. Pereira, and A. J. B. J. o. C. E. Dias, "Use of calcined layered double hydroxides for the removal of color and organic matter from textile

effluents: kinetic, equilibrium and recycling studies," *Brazilian Journal of Chemical Engineering*, vol. 31, no. 1, pp. 19-26, 2014.

[38] S. Li and J. J. C. S. R. Gong, "Strategies for improving the performance and stability of Ni-based catalysts for reforming reactions," *Chemical Society Reviews*, vol. 43, no. 21, pp. 7245-7256, 2014.

[39] G. Moradi, F. Khezeli, H. J. J. o. N. G. S. Hemmati, and Engineering, "Syngas production with dry reforming of methane over Ni/ZSM-5 catalysts," J*ournal of Natural gas Engineering*, vol. 33, pp. 657-665, 2016.

[40] G. Ertl, H. Knözinger, and J. Weitkamp, *Handbook of heterogeneous catalysis*. Citeseer, 1997.

[41] R. Dębek *et al.*, "Methane dry reforming over hydrotalcite-derived Ni–Mg–Al mixed oxides: the influence of Ni content on catalytic activity, selectivity and stability," *Catalysis Science & Technology*, vol. 6, no. 17, pp. 6705-6715, 2016.

[42] Z. Ma and F. J. S. s. r. Zaera, "Organic chemistry on solid surfaces," vol. 61, no. 5, pp. 229-281, 2006.

[43] B. Yousaf, "Hydrotalcite based ni-co bi-metallic catalysts for steam reforming of methane," NTNU, 2016.

[44] H. Wang, S. Yan, S. O. Salley, and K. S. J. F. Ng, "Support effects on hydrotreating of soybean oil over NiMo carbide catalyst," *Fuel*, vol. 111, pp. 81-87, 2013.

[45] H. M. McNair, J. M. Miller, and N. H. Snow, *Basic gas chromatography*. John Wiley & Sons, 2019.

[46] A. P. Tathod, O. M. J. C. G. Gazit, and Design, "Fundamental insights into the nucleation and growth of Mg–Al layered double hydroxides nanoparticles at low temperature," *Crystal Growth and Design*, vol. 16, no. 12, pp. 6709-6713, 2016.

[47] A. H. Dam, "Bimetallic catalyst system for steam reforming," 2015.

[48] H. Long *et al.*, "Ni-Co/Mg-Al catalyst derived from hydrotalcite-like compound prepared by plasma for dry reforming of methane," J*ournal of Energy chemistry*, vol. 22, no. 5, pp. 733-739, 2013.

[49] M. Bellotto, B. Rebours, O. Clause, J. Lynch, D. Bazin, and E. J. T. J. o. P. C. Elkaïm, "A reexamination of hydrotalcite crystal chemistry," *The Journal of Physical chemistry*, vol. 100, no. 20, pp. 8527-8534, 1996.

[50] X. Ge, M. Li, and J. J. J. o. S. S. C. Shen, "The reduction of Mg–Fe–O and Mg–Fe–Al–O complex oxides studied by temperature-programmed reduction combined with in situ

Mössbauer spectroscopy," J*ournal of Solid State chemistry,* vol. 161, no. 1, pp. 38-44, 2001.

[51] D. Li, M. Koike, L. Wang, Y. Nakagawa, Y. Xu, and K. J. C. Tomishige, "Regenerability of hydrotalcite-derived nickel–iron alloy nanoparticles for syngas production from biomass tar," *ChemSusChem,* vol. 7, no. 2, pp. 510-522, 2014.

[52] L. Smoláková, K. Frolich, I. Troppová, P. Kutálek, E. Kroft, and L. Čapek, "Determination of basic sites in Mg–Al mixed oxides by combination of TPD-CO2 and CO2 adsorption calorimetry," *Journal of Thermal Analysis and Calorimetry,* vol. 127, no. 3, pp. 1921-1929, 2017/03/01 2017.

[53] W. Y. Hernández, F. Aliç, A. Verberckmoes, and P. Van Der Voort, "Tuning the acidic–basic properties by Zn-substitution in Mg–Al hydrotalcites as optimal catalysts for the aldol condensation reaction," *Journal of Materials Science,* vol. 52, no. 1, pp. 628-642, 2016.

[54] J. Di Cosimo, V. Dıez, M. Xu, E. Iglesia, and C. J. J. o. C. Apesteguıa, "Structure and surface and catalytic properties of Mg-Al basic oxides," *Journal of catalysis*, vol. 178, no. 2, pp. 499-510, 1998.

[55] J. J. J. o. C. Di Cosimo, "Apesteguı, amp, CR´a, MJL Ginés and E. Iglesia," vol. 190, pp. 261-275, 2000.

[56] S. M. Kim *et al.*, "Cooperativity and dynamics increase the performance of NiFe dry reforming catalysts," *Journal of the American chemical Society,* vol. 139, no. 5, pp. 1937-1949, 2017.

[57] A. Tsoukalou, Q. Imtiaz, S. M. Kim, P. M. Abdala, S. Yoon, and C. R. J. J. o. C. Müller, "Dry-reforming of methane over bimetallic Ni–M/La2O3 (M= Co, Fe): The effect of the rate of La2O2CO3 formation and phase stability on the catalytic activity and stability," *Journal of Catalysis,* vol. 343, pp. 208-214, 2016.

APPENDIX: CALCULATIONS FOR CATALYSIS PREPARATION

The general formular for hydrotalcite-derived catalyst is $[M^{2+}{}_{1-x}\ M^{3+}{}_{x}(OH)_2]\ [(A^{n-}{}_{x/n}).mH_2O]$

Where: M^{2+}, M^{3+} - di and trivalent cations

A – interlayer anions

x – mole fraction of trivalent cations

After calcination and reduction, the composition of the catalyst becomes Ni-Fe/MgO-Al_2O_3

To calculate their respective compositions, let

a - mol of Ni^{2+}, *b* - mol of Mg^{2+}, *c* - mol of Fe^{3+}, *d* - mol of Al^{3+}

- If $\frac{M^{2+}}{M^{3+}} = 3$, then $\frac{a+b}{c+d} = 3$

To obtain pure hydrotalcite, the mole fraction of the trivalent cations must be between 0.2 and 0.33. Therefore, taking the average, x = 0.25

Then, a + b = 0.75

c + d = 0.25

- If the weight fraction of nickel is kept constant at 20%

Weight fraction of nickel = $\frac{mass\ of\ nickel}{total\ mass\ of\ the\ catalyst} = \frac{m_{Ni}}{m_{Ni}+m_{Mg}+m_{Fe}+m_{Al}} = \frac{a\times M_{Ni}}{a\times M_{Ni}+b\times M_{Mg}+c\times M_{Fe}+\frac{d}{2}\times M_{Al}}$

- $R = \frac{n_{Fe^{3+}}}{n_{Ni^{2+}}} = \frac{c}{a} = \{0.05, 0.1, 0.15, 0.2, 0.25, 0.3\}$
- $0.2 = \frac{a\times M_{Ni}}{a\times M_{Ni}+(0.75-a)\times M_{Mg}+Ra\times M_{Fe}+(\frac{0.25-Ra}{2})\times M_{Al}}$

After expanding the equation above,

$$a = \frac{0.15\times M_{MgO} + 0.025\times M_{Al_2O_3}}{0.8\times M_{Ni} - 0.2R\times M_{Fe} + 0.2\times M_{MgO} + 0.1R\times M_{Al_2O_3}}$$

The table below shows the stoichiometric coefficients of the hydrotalcite-derived catalyst.

Catalyst	Ni^{2+}	Fe^{3+}	Mg^{2+}	Al^{3+}	OH^-	CO_3^{2-}
CAT-0.05	0.1564	0.00782	0.5936	0.2422	2	0.125
CAT - 0.1	0.1565	0.01565	0.5935	0.23435	2	0.125
CAT - 0.15	0.1566	0.02349	0.5934	0.22651	2	0.125
CAT - 0.2	0.1568	0.03136	0.5932	0.21864	2	0.125
CAT - 0.25	0.1569	0.039225	0.5931	0.210775	2	0.125
CAT - 0.3	0.1571	0.04713	0.5929	0.20287	2	0.125

Catalyst	Mass of the chemicals needed to prepare the catalyst in grams					
	$Ni(NO_3)_2.6H_2O$	$Fe(NO_3)_3.9H_2O$	$Mg(NO_3)_2.6H_2O$	$Al(NO_3)_3.9H_2O$	NaOH	Na2CO3
CAT- 0.05	4.5471	0.3150	15.2221	9.0850	8.0000	2.6498
CAT - 0.1	4.5511	0.6306	15.2186	8.7912	8.0000	2.6498
CAT - 0.15	4.5552	0.9468	15.2150	8.4969	8.0000	2.6498
CAT - 0.2	4.5592	1.2635	15.2114	8.2020	8.0000	2.6498
CAT - 0.25	4.5633	1.5807	15.2079	7.9067	8.0000	2.6498
CAT - 0.3	4.5673	1.8987	15.2043	7.6108	8.0000	2.6498

Concentration of metal nitrate solution: 1M

Volume used in calculation: 500ml.